Conditional Moment Closure for Methane Oxidation Using Two Conditional Variables and Stochastic Processes

by

Jorge R. Lozada-Ramírez

B.A.Sc., Universidad de las Américas-Puebla, México, 1998

A THESIS SUBMITTED IN PARTIAL FULFILMENT OF
THE REQUIREMENTS FOR THE DEGREE OF

MASTER OF APPLIED SCIENCES

in

The Faculty of Graduate Studies

(Department of Mechanical Engineering)

We accept this thesis as conforming
to the required standard

THE UNIVERSITY OF BRITISH COLUMBIA

June 16, 2004

Library Authorization

In presenting this thesis in partial fulfillment of the requirements for an advanced degree at the University of British Columbia, I agree that the Library shall make it freely available for reference and study. I further agree that permission for extensive copying of this thesis for scholarly purposes may be granted by the head of my department or by his or her representatives. It is understood that copying or publication of this thesis for financial gain shall not be allowed without my written permission.

Jorge R. Lozada-Ramirez
Name of Author (*please print*)

_22/06/2004_
Date (dd/mm/yyyy)

Title of Thesis: _Conditional Moment Closure for Methane Oxidation Using Two Conditional Variables and Stochastic Processes_

Degree: _MASc_   Year: _2004_

Department of _Mechanical Engineering._
The University of British Columbia
Vancouver, BC   Canada

Abstract

'Conditional Moment Closure for Methane Oxidation Using Two Conditional
Variables and Stochastic Processes'

by Jorge R. Lozada-Ramírez

The conditional moment closure method using two conditioning scalar variables is applied to derive the transport equation of species mass fraction, temperature, and scalar dissipation in a decaying, isotropic, homogeneous turbulent methane-air flow. The strain tensor in the transport equation of scalar dissipation of the conditioning variables is simulated using stochastic processes. The results of this model are then compared to DNS and conditional moment closure with one variable for the same test case.

Contents

List of Figures

Nomenclature

A	Deterministic coefficient, amplitude of periodic force
a	Conditioning variable a
B	Deterministic coefficient
C	Constant
c	Speed of sound, concentration
C_p	Constant pressure specific heat
D	Molecular diffusivity, dimension
dW	Wiener process
E	Activation energy
F	Fuel, a stochastic process
g	Gravitational force
h	Specific enthalpy
I	Intermediates
J	Diffusion of energy, molecular diffusion
k	Arrhenius constant, reaction rate coefficient, energy level in coupled map lattice
L	Length
l	Length
Le	Lewis number
m	Mass
O	Oxidiser
P	Products
p	Pressure
Pr	Prandtl number
R^o	Ideal gas constant
Re	Reynolds number

$\dot{S}$	Surface stretch rate
Sc	Schmidt number
S_{ij}	Strain tensor
t	Time
u	Velocity
V	Volume
v	Velocity
W	Molecular mass
X	Mole fraction, stochastic variable
x	Coordinate axis
Y	Mass fraction, stochastic variable
Z	Mixture fraction

Greek Letters

α Value of the conditioning variable a

Γ Diffusion

γ Parameter in the coupled map lattice, ratio of specific heats

δ_{ij} Kronecker delta

ϵ Dissipation of turbulent kinetic energy

ζ Value of the conditioning variable Z

η Characteristic length microscale

Θ Product of the gradients of scalar dissipation

θ Random phase shift

κ Turbulent kinetic energy

λ Parameter in the coupled map lattice

μ Viscosity

ν Kinematic viscosity, stoichiometric coefficients

Π Product

ρ Density

Σ Summation

τ Characteristic time microscale, parameter in the coupled map lattice

τ_{ij} Viscous tensor

υ Characteristic velocity microscale

Φ Gradient squared of the conditioning variables

χ Scalar dissipation

Ψ A scalar field, periodic force with random phase shifting

$\dot{\omega}$ Chemical source term

ω Period of force

Acknowledgements

The work presented in this thesis was made possible thanks to the support and encouragement of many people. I would like to express my utmost appreciation to my supervisor, Dr. Kendal Bushe, for his patience and timely, expert advice. Thanks are also due to Dr. Andrea Frisque for her constant encouragement and for those long discussions regarding stochastic processes. The financial support of Mexico's National Council of Science and Tecnology *(CONACyT)* and of Westport Innovations, Inc. are also gratefully acknowledged.

Thanks are also given to Colin Blair, Andrea, and Ray Grout for proof-reading preeliminary drafts of this thesis and for their always insightful discussions on combustion, turbulence, modelling, programming, and politics. Thanks also go to Colin and Jen Bruce for their unconditional support and for becoming my family away from home.

Special thanks are due to Mina Halpern for her continuous support, encouragement, and motivation in reaching this goal. Thank you, Mina, for all those smiles in the times of hardship.

Finally, I would like to dedicate this thesis to my parents Jorge and Tere, and to my siblings Daniel and Raquel for always believing in me. Papá, Mamá, Dany y Raque; muchas gracias por su apoyo y por sus oraciones. Este documento está dedicado a ustedes como un pequeño tributo a su confianza y amor. Gracias por creer en mí.

Jorge R. Lozada-Ramírez   June, 2004

Chapter 1

Introduction

The complexity of the transport equations that describe turbulent combustion makes necessary the use of averaging procedures so that practical problems can be analyzed numerically in an efficient, timely fashion. This averaging process creates a *closure* problem by generating terms which are not explicit functions of the averaged variables [2]. Generally speaking, closure problems are solved by modelling the unclosed terms through the use of theoretical or empirical hypotheses or experimental results. In the following chapters of this thesis, a closure method for the transport equations of turbulent combustion will be formulated. The results obtained from the computational implementation of the resulting model on a decaying, isotropic, homegeneous, non-premixed turbulent flow of methane and air will be shown and compared to a reference DNS database of a similar flow.

1.1 Objective

The main objective of this research project is to explore the application of stochastic processes to the modelling of the strain tensor in the scalar dissipation transport equation that is derived using the Doubly Conditional Moment Closure (DCMC) method. The resulting system of equations is used to simulate the oxidation of methane by air in decaying, homogeneous, isotropic turbulence. It is expected that the predictions of species mass fractions and temperature will compare well with those obtained from a direct numerical simulation database and show an improvement over the results provided by a singly conditional moment closure simulation of the same test case.

1.2 Doubly Conditional Moment Closure (DCMC)

The Conditional Moment Closure (CMC) of Klimenko [3] and Bilger [4] was developed with the purpose of finding closure for the chemical source term of the species mass fraction transport

equation. This method is based on the assumption that the fluctuations of scalars, such as the chemical species mass fraction and temperature, are related to variations of other scalars. In this thesis, the CMC method has been expanded by using two different conditioning scalar variables. One of those variables, mixture fraction, is used to express the degree of mixedness of two or more elements in a non-premixed, reacting flow. A second non-reactive scalar variable named a has been defined to capture the effects of fluctuations due to strain along isosurfaces of mixture fraction. Through the use of the doubly conditional moment closure (DCMC) methodology, macro-mixing phenomena can be decoupled from the chemistry, while conserving the effects of micro-mixing via the scalar dissipation term.

1.3   Stochastic Processes

The strong coupling between fluid dynamics and chemistry in turbulent reacting flows is frequently modelled using the scalar dissipation term for which a number of different models have been proposed in the past. In this thesis, a transport equation is used to calculate scalar dissipation. This transport equation includes the strain tensor which is often modelled in turbulence research. Recognizing the chaotic behaviour of turbulence, the use of two stochastic processes to model the strain tensor in the transport equation of scalar dissipation term is proposed and analyzed. Stochastic processes are events that depend on stochastic variables that exhibit an unpredictable behaviour. In the first model, a periodic force with random phase shift (PF) is used to emulate the chaotic behaviour of the strain tensor. The second model uses the Coupled Map Lattice (CML) of Beck [5] and Hilgers and Beck [6], [7] that generates realisations of the fluctuating velocity increments as a function of time for a fully-developed turbulent flow. The strain tensor is then calculated using those velocity increments. The results from both codes are then compared to the Direct Numerical Simulation database of Bushe et al [8] and the CMC results of Bushe and Bilger [9].

1.4   Thesis Outline

In this chapter, the fundamental grounds and motivation for this research project have been discussed.

In Chapter 2, the fundamentals of combustion and turbulence, as well as turbulent com-

bustion, are addressed. The transport equations that describe turbulent combustion, as well as current turbulent combustion models, are also described.

In Chapter 3, the DCMC equations are derived. The closure assumptions and modelling of the strain tensor and of scalar dissipation are also discussed in this chapter.

Chapter 4 pertains to the implementation of the equations and models discussed in Chapter 3 to a decaying, homogeneous, isotropic turbulent reacting flow. The turbulence model and chemical kinetic mechanism used for this project are addressed and compared with a direct numerical simulation.

Finally, in Chapter 5, the conclusions about the research are articulated and recommendations made for future research.

Chapter 2

Combustion, Turbulence, and Stochastic Processes

Combustion can be defined as the self-sustaining process through which two or more compounds, fuels and oxidizer, are modified through a chemical reaction with an associated release of energy. The study of combustion phenomena implies a combination of thermodynamics, fluid mechanics/dynamics, chemical kinetics, and transport phenomena. Combustion processes can be classified according to the mixing behavior and the flow velocity regime of the system. Premixed systems and non-premixed systems can exist in both the laminar and turbulent regimes of fluid flow. This research utilizes mathematical modelling and computer simulation of combustion in a deacying, isotropic, homogeneous, non-premixed turbulent flow of air and methane. The Doubly Conditional Moment Closure (DCMC) method has been used to solve the transport equations of mass fraction of species. It is proposed to use a stochastic process to model the strain tensor in the transport equation of scalar dissipation responsible for the micro-mixing of species. Different options for the stochastic process are discussed.

2.1 Premixed Combustion

Premixed combustion occurs if the fuel and oxidizer are completely mixed before the chemical reaction takes place. Examples of premixed combustion are Bunsen burners and spark-ignition engines. Premixed combustion is often characterized by the burning velocity, which is a function of the chemical composition, initial temperature, and pressure of the premixed flow.

2.2 Non-premixed Combustion

In non-premixed combustion, the fuel and oxidizer are fed into a combustion chamber or reactor from different sources. Practical examples of non-premixed combustion include diesel engines, gas turbines and gas stoves. Unlike premixed combustion, where mixing has already taken place before the chemical reaction occurs, and the fuel/air ratio is homogeneous in the domain, in non-premixed combustion fuel and oxidizer have to mix in order for the reaction to proceed. The state of mixedness of the reactants is characterized by mixture fraction, which is defined as:

$$Z(x_i, t) \equiv \frac{Y(x_i, t) - Y_O}{Y_F - Y_O}.$$

Here, Y_F and Y_O are defined as the mass fractions of the fuel and oxidizer, respectively. Mixture fraction for the fuel stream is, $Z(x_i, t) = 1$, and $Z(x_i, t) = 0$ for the oxidizer stream.

2.3 Transport Equations

In general, the transport equations used in combustion express the coupling between the fluid mechanical and chemical reaction phenomena taking place in the combustion event. When dealing with reactive mixtures of gases, for example, the transport equations are usually derived making use of the kinetic theory of gases in order to capture the specific behavior of the system under study. Unless noted otherwise, the following equations are derived for their application to problems involving ideal gases.

2.3.1 Transport of Mass, Momentum, and Energy

The transport of mass balances the amount of mass entering and leaving any given control volume.

$$\frac{\partial \rho}{\partial t} + \frac{\partial \rho u_i}{\partial x_i} = 0.$$

The equation of transport of momentum indicates the change in momentum caused by the external forces (e.g. inertial, pressure, viscous, and body forces) acting on the fluid as,

$$\frac{\partial \rho u_i}{\partial t} + \frac{\partial \rho u_i u_j}{\partial x_j} = -\frac{\partial p}{\partial x_i} + \frac{\partial \tau_{ij}}{\partial x_i} + \rho g_i,$$

where the viscous tensor for a Newtonian fluid, using the molecular viscosity, μ_l, and the Kronecker delta δ_{ij}, is described by:

$$\tau_{ij} = \mu_l \left(\frac{\partial u_i}{\partial x_j} + \frac{\partial u_j}{\partial x_i} \right) - \frac{2}{3} \mu_l \delta_{ij} \left(\frac{\partial u_k}{\partial x_k} \right).$$

The equation of transport of energy balances the thermal, chemical, and kinetic energy of the system. Following Veynante and Vervisch [10], the transport equation of energy can be expressed in terms of the total specific enthalpy, $h_t = h + \frac{u_i^2}{2}$, of the system as follows:

$$\frac{\partial \rho h_t}{\partial t} + \frac{\partial \rho u_i h_t}{\partial x_i} = \frac{\partial p}{\partial t} + \frac{\partial}{\partial x_i} \left(J_i^h + u_j \tau_{ij} \right) + u_i \rho g_i$$

where the diffusion of energy, in this case of specific enthalpy, is described by the Fourier Law, as:

$$J_i^h = -\frac{\mu_l}{Pr} \left[\frac{\partial h}{\partial x_i} + \sum_{k=1}^{N} \left(\frac{Pr}{Sc_I} - 1 \right) h_k \frac{\partial Y_I}{\partial x_i} \right],$$

Here:

1. The Prandtl number, $Pr = \frac{\mu_i C_p}{\lambda}$, is the non-dimensional group that measures the ratio of transport of momentum due to diffusion to the temperature. C_p is the specific heat at constant pressure and λ is the thermal conductivity.

2. Sc_I, the Schmidt number of the Ith species, is defined as $Sc_I = \frac{\mu_l}{\rho D_I}$, where D_I is the diffusivity of the Ith species relative to a major or reference species.

3. Y_I is defined as the mass fraction of the Ith species, as $\frac{m_I}{m}$.

2.3.2 Transport of Mixture Fraction

Mixture fraction is a conserved scalar. It is only used to keep track of the mixing process as it evolves in time and in space.

$$\frac{\partial \rho Z}{\partial t} + u_i \frac{\partial \rho Z}{\partial x_i} - \frac{\partial}{\partial x_i} \left(\rho D_Z \frac{\partial Z}{\partial x_i} \right) = 0. \tag{2.1}$$

2.3.3 Transport of Species Mass Fraction

The transport equation of the mass fractions for $I = 1...N$ chemical species consists of accumulation, advection, diffusion, and production terms:

$$\frac{\partial \rho Y_I}{\partial t} + u_i \frac{\partial \rho Y_I}{\partial x_i} = -\frac{\partial J_i^I}{\partial x_i} + \dot{\omega}_I. \tag{2.2}$$

Using Fick's Law of diffusion [2], the molecular diffusion of species is defined as:

$$J_i^I \equiv -\rho D_I \frac{\partial Y_I}{\partial x_i}.$$

(2.3)

2.4 Chemical Kinetics and Reaction Mechanisms

The chemical source term, $\dot{\omega}_I$, in Eq. (2.2) describes the net rate of production of species due to chemical reactions. The chemical source term for M reactions is defined as [11],

$$\dot{\omega}_I = W_I \sum_{K=1}^{M} \left(\nu_{I,K}'' - \nu_{I,K}' \right) k \prod_{J=1}^{N} \left(\frac{X_J p}{R^\circ T} \right)^{\nu_{J,K}'},$$

(2.4)

where W_I is defined as the molecular mass of the Ith species. $\nu_{I,K}'$ and $\nu_{I,K}''$ are the stoichiometric coefficients in the Kth chemical reaction,

$$\sum_{I=1}^{N} A_I \nu_{I,K}' \rightleftharpoons \sum_{I=1}^{N} A_I \nu_{I,K}'',$$

with A_I being the chemical symbol of the Ith species in the chemical reaction. k is the Arrhenius type constant of the form,

$$k = BT^\alpha exp\left(-\frac{E}{R^\circ T} \right).$$

(2.5)

Here, $B_K T^{\alpha_K}$ corresponds to the frequency factor for the Kth reaction step, α_K is used to define the temperature dependence of the frequency factor for the Kth reaction, while E_K represents the activation energy required by the Kth reaction to proceed, and R° being the universal gas constant. Finally, the mole fraction of the Ith species X_I is defined as,

$$X_I = \frac{Y_I/W_I}{\sum_{I=1}^{N} (Y_I/W_I)}$$

(2.6)

with the ideal-gas law,

$$pV = mR^\circ T,$$

(2.7)

and,

$$m = \rho \sum_{I=1}^{N} (Y_I/W_I).$$

(2.8)

Substituting Eq. (2.8) into Eq. (2.7) leads to,

$$pV = R^0 T \rho \sum_{I=1}^{N} (Y_I/W_I).$$

(2.9)

Using Eqs. (2.5), (2.6), and (2.9), Eq. (2.4) can now be written as

$$\dot{\omega}_I = W_I \sum_{K=1}^{M} \left(\nu''_{I,K} - \nu'_{I,K} \right) B_K T^{\alpha_K} \exp \left(-\frac{E_K}{R^\circ T} \right) \prod_{J=1}^{N} \left(\frac{\rho Y_J}{W_J} \right)^{\nu'_{J,K}}. \tag{2.10}$$

The most basic analyses of combustion often rely on the assumption that the chemical reactions occur at faster rates than those associated to the transport phenomena occurring in the flow. This assumption is often referred to as 'fast chemistry' and usually denotes equilibrium states for chemical systems. By invoking fast chemistry, systems can be analyzed by using the basic laws of thermodynamics, which greatly simplifies the problem in hand. However, some chemical reactions occur at rates similar to those of transport processes; most transient phenomena like ignition, extinction, and re-ignition cannot be predicted with the use of fast chemistry. Kinetic mechanisms express the rates at which species are created or consumed during a chemical reaction. For a system of reactions $r = 1...R$ and species $s = 1...S$,

$$\sum_{s=1}^{S} \nu_{rs}^{(r)} A_s \xrightarrow{k_r} \sum_{s=1}^{S} \nu_{rs}^{(p)} A_s,$$

where k_r is the reaction rate coefficient, Eq. (2.5) and the stoichiometric coefficients of reactants, $\nu_{rs}^{(r)}$, and products $\nu_{rs}^{(p)}$. The rate of formation for the Ith species as a function of the concentration of S species, c_S, as given by Warnatz [2]:

$$\dot{\omega}_{I,r} = \left(\frac{\partial c_i}{\partial t} \right)_{chem,r} = k_r \left(\nu_{ri}^{(p)} - \nu_{ri}^{(r)} \right) \prod_{s=1}^{S} c_S^{\nu_{rs}^{(p)}}.$$

Reaction rates are strongly non-linear functions of temperature via the reaction rate coefficient k. Pressure is also known to affect the reaction rates by modifying the concentration of species.

Complex reaction mechanisms, e.g. for the oxidation of methane, can consist of many different global reactions. Researchers have proposed methods to reduce the number of reactions to include only those that are deemed most relevant for the study of the phenomena of interest. Most reduction processes are based on assumptions of partial equilibrium and quasi-steady state, which implies that reduced mechanisms are applicable only under certain limiting conditions. Peters [12], identified the reduction in computation time for the numerical simulation of combustion events, as well as the applicability of asymptotic methods to the analysis of flame structures as the two most important applications of reduced kinetic mechanisms. As an example, Bilger et al [13] proposed a method to derive a four-step mechanism

for a methane-air flame which is in good agreement with the more complex mechanisms from which it originated for a limited class of combustion problems. The reduced chemical kinetic mechanism used in this research project is described in Chapter 4.

2.5 Scales of Turbulence and Kolmogorov Scales

Turbulent flows can be found in different scales of magnitude ranging from large scales such as those found in oceans or atmospherically relevant scales, to the very small scales such as those studied in combustion. Turbulence is a high-energy phenomenon. This kinetic energy is later dissipated, mainly through viscosity. The effects of molecular viscosity, however, are relevant only at very small scales. This implies that, in order for the energy to be dissipated at those scales, this energy must be transferred from the largest scales down to the smaller scales. The vortices, also known as eddies, present in a turbulent flow vary in scale and they can be correlated to the development of velocity gradients. It has been found that the largest vortices are responsible for most of the transport of momentum. However, viscosity acting at molecular scales is responsible for the dissipation of energy through a conversion of kinetic energy into heat at the small scales of motion [14]. Since chemical reactions typically take place at this same molecular level, it is important to consider these small turbulence scales.

The K41 theory, proposed by Kolmogorov [15], states that, at the smallest scales of turbulence, the fluid motion is self-similar and isotropic, giving origin to the concept of universality of turbulence at such small scales. Following Kolmogorov, the use of the kinematic viscosity of the fluid, ν, and the energy dissipation rate normalised per unit mass, ϵ, permits the definition of the following microscales, also known as the Kolmogorov scales.

- Characteristic length microscale,

$$\eta = \left(\frac{\nu^3}{\epsilon}\right)^{\frac{1}{4}}$$

- Characteristic time microscale,

$$\tau = \left(\frac{\nu}{\epsilon}\right)^{\frac{1}{2}}$$

- Characteristic velocity microscale,

$$v = (\nu\epsilon)^{\frac{1}{4}}$$

At these microscales, the resulting local Kolmogorov Reynolds number is equal to unity, which means that there is no turbulence at smaller scales.

2.6   Cascade of Turbulent Kinetic Energy

Based on Kolmogorov's ideas, researchers have developed the concept of the energy cascade, which states that turbulent kinetic energy transfers from large to small scales via vortex stretching and once the energy reaches the smaller scales of turbulence, viscous dissipation occurs. Tennekes and Lumley [14] provide a complete discussion on the vortex-stretching mechanism. Fig. 2.1 (from Peters [1]) shows the turbulent kinetic energy spectrum as a function of wave number k, where k is the inverse of the vortex or eddy size. From this figure, it can be seen that the kinetic energy exhibits a monotonic decay in the logarithmic plot, with a slope of $-5/3$ along the inertial subrange. This is followed by an abrupt decay in the viscous subrange, where viscous dissipation affects the smallest scales of turbulence.
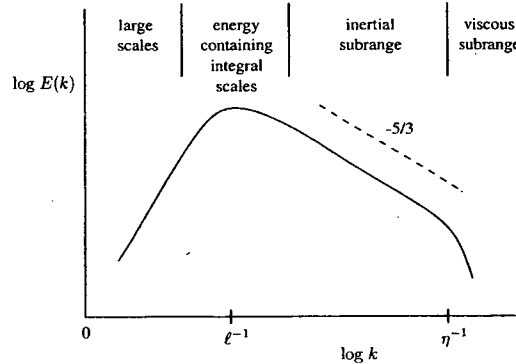
Figure 2.1: Turbulent kinetic energy spectrum, from Peters [1]

2.7   Turbulence Simulation and Modelling

The Navier-Stokes equations that describe turbulence can, in principle, be solved directly using numerical techniques. In reality, the strong coupling and non-linearity of the equations, along with the wide range of length and time scales involved in the solution and the chaotic nature of turbulence, make such direct calculations possible only in very limited cases. Time and mass averaging techniques have been developed to circumvent this problem. The introduction of such techniques, however, produces terms for which the solution is either not known or

cannot be expressed as an explicit function of the averaged variables. Oftentimes, these terms have to be modelled. The following sections describe the simulation and modelling techniques most widely used in turbulence.

2.7.1 Direct Numerical Simulation (DNS)

In direct numerical simulation (DNS), the Navier-Stokes equations are solved numerically. This requires very fine spatial and temporal discretisations so that the transport equations can be solved from the large scales down to the Kolmogorov microscales. In general, it is estimated that the computation time for a DNS simulation increases approximately at a rate of Re^4 [2]. Consequently, at present only low Reynolds number flows can be solved directly. This limitation prevents the use of DNS for most practical applications. Currently, most research using DNS is aimed at the analysis of small turbulent structures, and the development and validation of closure models.

2.7.2 Large-Eddy Simulation (LES)

With Large-Eddy Simulation (LES), the large scales of turbulence are calculated directly in the same way as in DNS. The smaller scales are modelled using turbulence models and through processes of numerical filtering. LES provides high-quality results at a much lower computational expense than DNS.

2.7.3 Time or Ensemble Averaging (Reynolds Decomposition)

The Reynolds decomposition [14], is frequently used to obtain statistical information from a turbulent flow. The time-average velocity of the flow can be defined as,

$$\overline{u}_i(x,t) = \int_0^T \frac{u_i(x,t)}{T} dt,$$

which can also be expressed as:

$$\overline{u}_i(x,t) = \frac{\sum_k^N u_i(x,t;k)}{N}$$

so that instantaneous fluctuations of velocity around the time-average mean can be expressed as,

$$u_i'(x,t) = u_i(x,t) - \overline{u}_i(x).$$

An important, and widely used parameter in turbulence characterization is the turbulent kinetic energy κ, which is obtained from taking the root mean square and time-averaging the velocity fluctuations as follows [16],

$$\overline{\kappa} = \frac{1}{2}\overline{u_i' u_i'},$$

which, for a three-dimensional flow field becomes,

$$\overline{\kappa} = \frac{\overline{u_1'^2} + \overline{u_2'^2} + \overline{u_3'^2}}{2}.$$

If no additional energy is transferred to the system, the kinetic energy dissipates in time at a rate given by,

$$\epsilon = \frac{D\kappa}{Dt}.$$

2.7.4 Turbulence Models

From probability theory, it can be shown that the ensemble average of the velocity fluctuations around the mean value is equal to zero [14], or in mathematical form $\langle u_i' \rangle = 0$. The second moment $\langle u_i' u_i' \rangle$ that represents the statistical correlation between u_i and u_j becomes an extra unknown in the system of equations for which an equation as an explicit function of the averaged variables is not available. This is commonly known as a *closure* problem and the *unclosed* terms are often modelled using physical or mathematical tools.

Launder and Spalding [17], and Pope [18] summarise different mathematical turbulence models. Those models range from one-equation to multi-equation mathematical expressions to characterise turbulent phenomena and were derived as an alternative to previous models such as the mixing-length model. The numerical designation for the models is based on the number of partial differential equations which are needed to calculate the modelled parameters. Gatski and Rumsey [19], for example, identified variations of previous models that have originated 'zero-equation' models, which are algebraic relations to define the vortical or eddy viscosity, and 'half-equation' models where an ordinary differential equation is solved to calculate the eddy viscosity. Results obtained from zero- to multi-equation models may vary considerably, due to the different degrees of complexity and detail that they may include in their analyses. Most models are derived for specific applications, e.g. flow around a cylinder, boundary-layer flows, and so forth and they are usually tuned to provide acceptable to good approximations to experimental results.

2.8 Turbulent Combustion

Most practical applications involving combustion occur in turbulent regimes. Directly or indirectly, all of the characteristics of turbulence have a major effect on the evolution of a combustion event. Vorticity, for example, increases the interface area between fuel and oxidiser in non-premixed combustion, or between reactants, intermediates, and products in premixed flames, which results in an increased rate of reaction.

In premixed combustion, turbulence has several important effects. It increases the area of the reactant-intermediate-products interface, which in turn increases the rate of reaction. This increase in area is due to the appearance of 'wrinkles' in the flame front which are produced by the action of turbulent vortices. As a consequence of this stretching, the reaction zone becomes thinner, promoting higher flame-propagation velocities. If the accelerated mixing rate produced by the stretch effect reaches a point where mixing takes place faster than reaction, extinction of the flame occurs [20].

In non-premixed combustion, the most significant role of turbulence is to enhance mixing. This is achieved through the increase in the surface area of the fuel-oxidiser interface due to the strain and stretch created by vorticity and the high diffusion velocity present in turbulent flows which is a result of an increase in gradients. Since non-premixed combustion is a primarily mixing-limited phenomenon, the result of these effects is of paramount importance.

2.9 Turbulent Combustion Simulation and Modelling

There are a number of different techniques and approaches to solve the equations that describe the evolution of a turbulent reacting flow. Well established methods have been used for the study and analysis of turbulence. These methods have been modified and adapted to account for the interactions between fluid mechanics/dynamics and chemistry. Basically, most of the research work is dedicated to closure methods for the chemical source term. The works by Mell et al [21], Swaminathan and Bilger [22], Bilger [23], and Peters [1], amongst others, offer a variety of options for the modelling of the chemical source term. A brief description of the most widely used techniques and their applications is given below.

2.9.1 DNS

Echekki et al [24] report the use of DNS, coupled with a multi-step chemical kinetics mechanism for the simulation of a 2-D premixed turbulent reacting flow. Papers by Bushe et al [8] and Swaminathan and Bilger [22] describe the use of DNS with reduced chemical kinetic mechanisms in the study of non-premixed combustion. The DNS database of the oxidation of methane in a turbulent flow of Bushe et al [8] is used as the baseline for the comparison with the results of the model developed in this thesis.

2.9.2 Favre Averaging

Combustion processes are characterized by considerable density fluctuations, which has prompted the development of the density-weighted, or Favre averaging. The Favre average of a property, such as mass fraction for example, can be defined as

$$\widetilde{Y} = \frac{\overline{\rho Y}}{\overline{\rho}} \tag{2.11}$$

The instantaneous local value of mass fraction can be defined in terms of its average and fluctuation as

$$Y(x,t) = \overline{Y}(x,t) + Y'(x,t) \tag{2.12}$$

Similarly, the instantaneous local value of mass fraction is defined in terms of its Favre average and fluctuation as

$$Y(x,t) = \widetilde{Y}(x,t) + Y''(x,t) \tag{2.13}$$

Combining the definition of Eq. (2.11) with Eq. (2.12) leads to an expression for the Favre average of mass fraction in terms of the average mass fraction as

$$\widetilde{Y} = \frac{\overline{(\overline{\rho} + \rho')(\overline{Y} + Y')}}{\overline{\rho}} = \overline{Y} + \frac{\overline{\rho' Y'}}{\overline{\rho}}. \tag{2.14}$$

The term $\rho' Y'$ in Eq. (2.14) denotes the correlation between the fluctuations of density and mass fraction. This is an unclosed term which can be computed using a transport equation, or modelled using theoretical or empirical relations.

2.9.3 LES

Chemical reactions occur at small scales where the flow is modelled in LES, not resolved; this implies the need for models for the chemical source term in the transport equations of mass

fraction of species [16]. LES results have been used as benchmarks for *a priori* testing of other simulations. The piloted flame of Pitsch and Steiner [25], as well as that of Steiner and Bushe [26], have been used in comparative studies of computer simulations. In the case of the work by Steiner and Bushe, LES was incorporated with the newly-developed conditional source-term estimation. Laurence [27] discussed applications of LES in industrial settings, and identified the ongoing work on numerical methods for finite volumes in unstructured grids as one of the main activities aimed at providing more opportunities to such applications of the method.

2.9.4   Laminar Flamelets

Flow visualisation of reacting flows with low-intensity turbulence shows that curved flame fronts propagate outwards from the source of ignition to the boundaries of the system. In this fashion, the turbulent flame can be conceptualised as an aggregation of such flame fronts. This is also known as the flamelet regime. Based on this concept, the Laminar Flamelets, as described by Peters [28], [1], are thin (their width being smaller than the Kolmogorov length-scale), reactive sheets that react and diffuse within a non-reactive field. This method assumes that once ignition has occurred, the chemical time scale is greatly accelerated, reducing the reaction zone into a thin sheet. This concept was further developed into assuming that if the thin reaction zone is smaller than the Kolmogorov length-scale, then the flow in that zone is laminar, due to the fact that there exists no turbulence below the Kolmogorov microscales.

Much research has been dedicated to the development of the flamelet model. Peters [1] provided a complete description of the model, as well as its formal application to premixed and non-premixed turbulent combustion. Lentini [29] explored the application of the stretched laminar flamelet method combined with the $\kappa - \epsilon$ model for turbulence in a turbulent non-premixed flow and reported good agreement with results obtained from experiments performed at the flamelet regime. Cook et al [30] presented the large-eddy laminar flamelet model in which the chemistry at the smaller scales was modelled using the flamelet theory. The flamelet model offers good predictions of the major chemical species that originate in combustion of hydrocarbon-based fuels at what is known as the 'flamelet regime'. However, the flamelet theory applies under very specific conditions of the flow, e.g. the flamelet thickness is smaller than

the smaller length-scales of turbulence, which limits the effective application of the flamelet method. Swaminathan and Bilger [22] pointed out that the flamelet model falls short of providing good predictions of the minor species in combustion of hydrocarbon fuels. This point was also discussed by Mell et al [21] when comparing the flamelet and the conditional moment closure (CMC) models with a DNS database for different flow configurations to study the effects of variations of scalar dissipation on flamelet and CMC results.

An improvement over the laminar flamelet model is the unsteady laminar flamelet theory, which introduces a Langrangian time frame that records the time dependence in the flame structure. Mauss et al [31] presented results that seem to indicate that the transient variations of the flamelet structure of a steady turbulent non-premixed flame are responsible for the scattering of experimental data points obtained with one-point Raman measurements. Pitsch [32] obtained good agreement between experiments and the results of the unsteady flamelet model for a turbulent non-premixed $CH_4/H_2/N_2$-air flame.

2.9.5   Probability Density Function (PDF) Modelling

In the PDF method, a transport equation for the joint PDF of relevant scalars is solved to model the evolution of a combustion event. These scalars can include mass fraction of chemical species, flow velocities, temperature, mixture fraction, and so forth. An important advantage of this method is that the chemical source term is solved for directly, without the need of a model. Modelling is necessary, however, for the molecular mixing terms in scalar space, as well as for the turbulent transport terms in physical space [33]. Due to the high-dimensionality inherent to this method, traditional computing techniques are insufficient. This has prompted researchers to apply numerical methods capable of dealing with problems with a large number of variables and dimensions, such as Monte Carlo methods. These applications will be reviewed with more detail in the following sections of this thesis.

2.9.6   Conditional Moment Closure

The Conditional Moment Closure (CMC) of Klimenko [3] and Bilger [4] determines closure for the chemical source term of the transport equation of the mass fraction of species. This method is based on the assumption that the fluctuations of scalars, such as mass fraction

of chemical species and temperature, are associated with variations of other scalars. The advantage of using the CMC method is that macromixing phenomena can be decoupled from the chemical kinetics, while conserving the effects of micromixing via the scalar dissipation term. The method is described and its equations derived in Chapter 3.

2.10 Stochastic Processes and Monte Carlo Methods

The theory behind stochastic processes originated from the observations of the trajectories of pollen particles moving on a water surface made by Brown in 1827 and later independently developed into an elegant mathematical theory by Einstein [34], [35], Smoluchowski [36], and Langevin [37]. The experiments by Perrin [38], [39], [40], [41], [42] confirmed the previous theoretical analyses and his work was awarded the Nobel Prize of Physics in 1926. The initial applications of the method concentrated on physics, mathematics and chemistry. Today, stochastic processes are extensively applied in fields such as biology, finance, economics, demography, atmospheric and ocean sciences, amongst many others. Different numerical methods, such as the Monte Carlo (MC) method, have been developed as tools for the study of stochastic processes. The MC method is intended to solve multi-dimensional problems with a large number of variables. This can be a very inefficient method when used to solve simple problems given the large number of computations required.

2.10.1 Monte Carlo Simulations of Turbulence

Kramer [43] reviewed the application of the MC method in generic turbulence problems. In this work, a thorough description of the two different (Eulerian and Lagrangian) types of MC simulation is presented. The MC method is remarkably useful for the simulation of turbulent flows given its ability to treat multi-dimensional problems with a large number of degrees of freedom. Another attractive feature of this method is its ability to generate chaotic particle trajectories and velocity field structures. In the Eulerian approach, a stochastic velocity field model replaces the turbulent velocity field to be simulated. This field is then solved in a spatial domain, which is computationally less demanding when compared to the solution of the Navier-Stokes partial differential equations. The stochastic field is tailored to the specific application and is frequently used to simulate trajectories of particles suspended in a flow.

A number of methods exist to numerically solve the equations derived using the Eulerian approach. The Fourier method is based on a spectral formulation for a homogeneous Gaussian stochastic field. A major drawback of this method is the generation of a spatial period that has detrimental effects on turbulent diffusion simulation. Using a randomization method, the stochastic Fourier integral is discretised by stochastic wave numbers. Despite the fact that this method provides useful data to simulate velocity fields with strong long-range correlations, those fields have non-Gaussian statistics. According to Elliot et al [44] and Sabelfeld [45] this limits the applications of this method for ideal mathematical or physical turbulence models. More physically meaningful models have also been developed. Among them are the moving-average and the wavelet methods. McCoy [46] introduced a Gaussian stochastic field represented in physical space using white noise convolved against a kernel. Long-range correlations in the velocity field can be appropriately simulated using the wavelet method. There exists a combination of Fourier-wavelet methods that present improvements over its precursors. This method has been reported to have shown excellent results when simulating velocity fields with the condition of self-similarity scaling of their structures.

A Lagrangian MC simulation utilises particles evolving in a stochastic model. All the effects of turbulence are incorporated within the properties of each particle. Despite the fact that the Lagrangian MC simulation does not make reference to a fluid velocity field, Minier and Pozorsky [47] and Welton [48] have used it to simulate the motion of a turbulent flow by analysing the stochastic evolution of a group of particles. The average properties of this group of particles (and of the ones in the vicinity of the target field) define the properties of the fluid, and of the flow, at that specific location. The methods developed to deal with MC simulations using the Lagrangian approach include the simulation of fluid motion and particles, the simulation of immersed bodies and hybrid LES/MC schemes.

In the simulation of fluid motion and particles, a set of fluid particles is followed according to a stochastic formulation. Physical, or pseudo-physical properties are defined for the particles. The evolution of the dynamics of the flow is assumed to be the average of the simulated particles. This method offers flexibility in the way that it can provide some insight into the mixing process of the unresolved scales of the turbulent flow by the use of a

simple Langevin formulation. If more details are desirable, the stochastic formulation must be changed. Stochastic differential equations in the form of Markov processes are often used with this purpose in mind [49]. The simulation of immersed bodies follows a similar procedure. Pozorsky and Minier [50] reported an approach in which two sets of stochastic particles are defined. The first set represents the immersed particles, while the second is intended to simulate the flow. The physical and pseudo-physical properties of both sets of particles are different from one another. A major drawback of these methods is that they can only simulate homogeneous turbulent flows.

In the hybrid LES/MC schemes the flow field is resolved using a LES formulation, while the mixing (and chemical reaction, if reacting flow is being considered) simulations are resolved using a MC formulation. This scheme calls for the continuous feedback from one formulation to the other. Jaberi et al [51] and Obliego et al [52] have reported an increase in accuracy in their LES calculations after the addition of the MC component. The apparent reason for this is that the MC simulation provides some information on the effects of the small scales otherwise neglected by the LES model. This model has also been used successfully in non-homogeneous turbulent flows, which extends its potential for applicability to more realistic problems. Le Maitre et al [53] proposed a method in which a stochastic spectral finite element method undertakes the formalism of a MC simulation and offered numerous results claiming improvements in computational expenses, amongst other advantages over the MC method. Unfortunately, this research group did not provide a comparison between the results of the two formulations.

2.10.2 Monte Carlo Simulations of Turbulent Reacting Flows

Most applications of the MC method in turbulent reacting flows follow one of the Lagrangian formulations described in the preceding section. Pope [54] described what appears to be the first application of the MC simulation to a turbulent reacting flow. This method has shown great usefulness given its capabilities of dealing with problems with a large number of variables and dimensions. Its first and foremost application is intended to numerically solve the PDF transport equations derived for a trubulent reacting flow.

The advantages of the method are numerous. As described in different papers [54], [55], the PDF method provides closure to the chemical source term in the equation without the need of any modelling and can be applied to either premixed or non-premixed flows. It is also known that this method incurs large computational demands, has no ability to model wall-type boundaries, and is difficult to apply in complex flows. According to Pope [54], the computational requirements of this method increase linearly with the number of variables used (in this case dimensions, as well), compared to the exponential increase of computations required by traditional finite-difference formulations. This fact provides a way of dealing with problems involving many species. As discussed in the previous section, the MC method can deal with the simulation of walls and complex, inhomogeneous flows, hence solving the more relevant drawbacks of the PDF method. As described by Pope [54], stochastic particles were used to mimic the chemical and thermodynamic properties of the flow. These particles, however, were defined as a numerical tool and have no physical meaning. A plug-flow reactor problem with imperfect mixing was simulated using the MC method, using a single scalar to model the concentration of reaction products. Pope's numerical results were in good agreement to those obtained in experiments performed by Batt [56].

Valiño [57] proposed an Eulerian MC formulation for the simulation of the PDF of a single scalar in a turbulent flow. His proposal was to use stochastic particles 'jumping' from node to node in the spatial domain according to specific rules (a stochastic equation). Hulek and Lindstedt [58] offered a comparison between data obtained from DNS and from MC simulations. Their formulation used the MC method to solve the terms modelled with the PDF method in the flamelet equation. This method, called flamelet acceleration, was also tested and it appeared to be an improvement when compared with the standard flamelet solution. Hulek and Lindstedt [59] later modelled premixed turbulent flames using PDF and MC methods. The MC simulation was used to solve the mass density function evolution equation. Stochastic particles evolved following deterministic processes representing the closed terms of the equation and stochastic processes designed to model the effect of the unclosed terms. They showed the comparison between several different numerical formulations and experimental results, where it can be seen that the PDF-MC simulations were in good agreement with experiments.

The special ability of the MC method to mimic turbulent mixing was explored by Kawanabe et al [60]. The methodology was applied to a plug-flow flame in unsteady turbulent combustion. The turbulence model used was a standard $\kappa - \epsilon$ and the mixture is forced to avoid homogeneity. Cannon et al [61] and Kraft and Fey [62] have explored stochastic reactor models using the PDF and MC methods. Cannon's group offered some practical results, while Kraft and Fey mainly developed a purely analytical solution to the stochastic reactor model. Cannon's research was aimed at the prediction of CO and NO in premixed combustion of methane, using a partially stirred reactor (PaSR). Conceptually, the PaSR could be thought of as a MC process itself, since it also randomly selects particles that are then forced to interact amongst themselves. This method is an improvement over the perfectly stirred reactor (PSR) since finite-rate mixing effects can be included in the solution. The mixing term was modelled using a deterministic method rather than a MC method. The good agreement between the 9-step simulation and the detailed kinetic solution demonstrated the robustness and accuracy of this particular model.

2.11 Summary

In this Chapter, the fundamentals of turbulent combustion, have been reviewed. Turbulence, scales of turbulence, and turbulence simulation and modelling were also treated, along with the interactions between turbulence and combustion. Descriptions of the regimes and equations that define turbulent combustion, as well as some of the most important analytical tools available for the solution of those equations were also presented in this chapter.

A detailed description of the applications of the Monte Carlo simulations in turbulence and turbulent combustion was provided. It has been observed that there exist a number of different options in which the MC method can be used to solve numerically demanding problems in turbulent combustion. Future possible applications include particulate matter and pollutant formation mechanisms and mass transport in permeable membranes. Of particular interest to this research is the capability of the method to be included to solve problems expressed in terms of different modelling theories such as conditional moment closure, LES, or flamelet models. An increasing number of research opportunities exist in this field, with promises of continuous and prolific growth in the near future.

Chapter 3

The DCMC Method with Stochastic Processes

Conditional moments are averages which are calculated for those members or realisations that satisfy some predefined condition. The conditional moment closure method (CMC), independently developed by Klimenko [3] and Bilger [4], provides closure for the chemical source term in the transport equation of species and enthalpy or temperature by assuming that the variability in temperature and the mass fractions of species can be linked to the fluctuations of a given scalar variable. The reaction progress variable and mixture fraction are common choices of scalar variables for premixed and non-premixed combustion analysis, respectively. If the mass fractions of species are expressed as functions of not only space and time, but also as functions of the conditioning variable, their conditional averages can then be used to approximate the conditional average of the source term as $\overline{\dot{\omega}|Z = \zeta} \approx \dot{\omega}\left(\overline{T|Z = \zeta}, \overline{Y_I|Z = \zeta}\right)$. The overbar in this notation indicates that the mean value has been calculated from averaging over $n = 1...N$ realisations. The vertical bar means 'given', and in the case of Y_I denotes the value of the mass fraction given that mixture fraction has a value of ζ.

As an illustration of the theoretical basis of the CMC method, Fig. 3.1 shows a plot of individual $n = 1...N$ realisations of a simulation of temperature (blue lines). Where the unconditional average of temperature, $\overline{T} = \sum_{i=1}^{N} T_i/N$, is represented by the horizontal line at around $T \approx 500$, and the red curve is the calculated conditional average of temperature, $\overline{T} = \langle T|Z = \zeta \rangle$, where the angle brackets indicate that only those realisations that comply with the condition of $Z = \zeta$ are considered in the averaging process. It is clear from Fig. 3.1 that the information obtained from conditional averages is more representative of the actual relationship between T and Z than that obtained from unconditional averages.
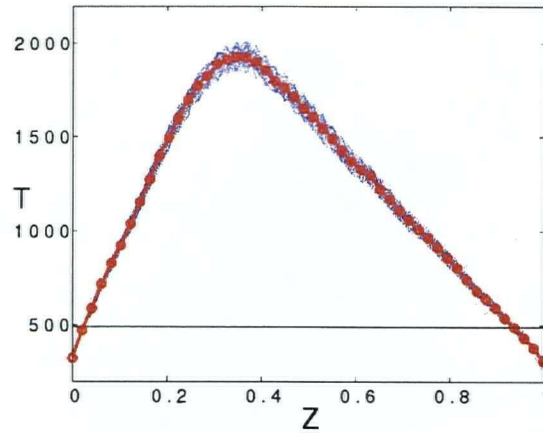
Figure 3.1: Conditional average of temperature; blue(.) DNS, red(-) $\langle T|Z \rangle$, black(-) $\overline{T}$

Researchers have previously explored the application of the CMC method and have found that using only one conditional variable offers good results in terms of species mass fraction and temperature predictions. However, the presence of triple flames and prediction of ignition, extinction, and re-ignition phenomena are not well reproduced by just one conditioning variable. Figure 3.2, from Bushe et al [8], shows a slice of a 3-dimensional DNS calculation of temperature. The contour lines represent isopleths of mixture fraction, which were formed by the intersection of the slicing plane and the corresponding isosurfaces of mixture fraction. The white isopleth corresponds to the stoichiometric mixture fraction.
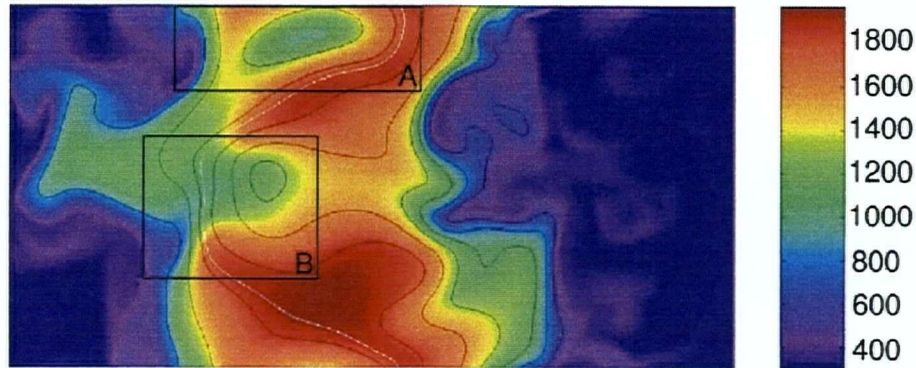

Figure 3.2: DNS calculation of temperature, from Bushe [8]

It is clear that this temperature field exhibits strong fluctuations in regions of constant mixture fraction. This is evident in the 'cold pockets' shown in regions A and B in the figure. These cold zones are typical of extinguishing flames. From this figure, it can also be

observed that there is a transition between hot zones, located to the right of region B. This transition could correspond to re-ignition or bifurcation of the flame. It has been proposed that using a second conditional variable would solve those issues [9], [16], [63]. This result is of paramount importance, given the close relationship between these phenomena and the formation of pollutants. In this thesis, the use of two conditioning variables has been explored. One variable is mixture fraction Z, which characterises the state of mixedness of the flow for a given instant in time and space. The other conditional variable is named a and is introduced to capture fluctuations along an isosurface of mixture fraction. This is achieved through the definition of the scalar a as a conserved scalar with a spatial gradient perpendicular to that of mixture fraction.

3.1   Conditional Moment Closure with Two Conditional Variables (DCMC)

The use of a second conditional variable has been proposed as a way to solve the shortcomings of the original CMC method. Bushe [16] used a second conditioning variable that filtered between regions of a surface defined by a constant mixture fraction, hence detecting differences in the stretch rate history of the flow. The results of a simulation of auto-ignition of n-Heptane showed an improvement over the single-conditional method in detecting autoignition and double flames when compared to DNS databases. However, the same results failed to show the presence of triple flames present in the reference data. Cha et al [63] used the scalar dissipation rate as the second conditioning variable for the simulation of a methane-air turbulent reacting flow. After comparing their results with those obtained from an experimental jet and a DNS simulation, it was found that there exists good agreement in the prediction of extinction phenomena, but they obtained an early prediction of the onset of re-ignition. High fluctuations around the conditional means, specifically for low values of the scalar dissipation rate, were identified as a possible source for the discrepancies with the reference data.

3.2   Derivation of the DCMC Equations

During the development of this project, two conditioning conditional variables have been used.

- Mixture fraction $Z = Z(x_i, t)$,

- and $a = a(x_i, t)$.

These two random variables are related to the non-random variables ζ and α using:

$$\overline{\dot{\omega}|(Z = \zeta, a = \alpha)} \approx \dot{\omega}\left(\overline{T|(Z = \zeta, a = \alpha)}, \overline{Y_I|(Z = \zeta, a = \alpha)}\right), \qquad (3.1)$$

such that the result is a function of what values are chosen for the conditioning variables ζ and α.

The definition of the conditional average of the mass fraction of the Ith species is

$$\overline{Y_I} = \overline{Y_I}(\zeta, \alpha; x_i, t) \equiv \langle Y_I(x_i, t) | Z(x_i, t) = \zeta, a(x_i, t) = \alpha \rangle,$$

so that the instantaneous value of species mass fraction using conditional average and fluctuations around that mean can be expressed as

$$Y_I(x_i, t; n) = \overline{Y_I|_{Z(x_i, t; n), a(x_i, t; n)}} + Y_I'.$$

Eq. (2.3) is substituted in Eq. (2.2) to obtain a new version of the transport equation of species mass fractions as

$$\frac{\partial \rho Y_I}{\partial t} + \frac{\partial \rho u_i Y_I}{\partial x_i} = \frac{\partial}{\partial x_i}\left(\rho D_I \frac{\partial Y_I}{\partial x_i}\right) + \dot{\omega}_I. \qquad (3.2)$$

Using the experimental results from Vargaftik [64], it has been proposed [16] that $\rho D_I = $ constant, and that $D_Z = D_I$, implying that $Le = 1$. Using these assumptions, Eq. (3.2) can be written as

$$\frac{\partial Y_I}{\partial t} + u_i \frac{\partial Y_I}{\partial x_i} - D \frac{\partial^2 Y_I}{\partial x_i \partial x_i} = \frac{\dot{\omega}_I}{\rho}. \qquad (3.3)$$

To express Eq. (3.3) in terms of conditional averages, it is required to derive partial derivatives, which were obtained by applying the chain rule of differential calculus.

- The partial derivative of species mass fraction with respect to time is

$$\frac{\partial Y_I}{\partial t} = \frac{\partial \overline{Y_I}}{\partial t} + \frac{\partial \overline{Y_I}}{\partial \zeta}\frac{\partial Z}{\partial t} + \frac{\partial \overline{Y_I}}{\partial \alpha}\frac{\partial a}{\partial t} + \frac{\partial Y_I'}{\partial t}. \qquad (3.4)$$

- The first partial derivative of species mass fraction with respect to space is

$$\frac{\partial Y_I}{\partial x_i} = \frac{\partial \overline{Y_I}}{\partial x_i} + \frac{\partial \overline{Y_I}}{\partial \zeta}\frac{\partial Z}{\partial x_i} + \frac{\partial \overline{Y_I}}{\partial \alpha}\frac{\partial a}{\partial x_i} + \frac{\partial Y_I'}{\partial x_i}. \qquad (3.5)$$

- The second partial derivative of species mass fraction with respect to space is

$$
\begin{aligned}
\frac{\partial^2 Y_I}{\partial x_i \partial x_i} &= \frac{\partial^2 \overline{Y_I}}{\partial \zeta^2} \frac{\partial Z}{\partial x_i} \frac{\partial Z}{\partial x_i} + \frac{\partial^2 \overline{Y_I}}{\partial \alpha^2} \frac{\partial a}{\partial x_i} \frac{\partial a}{\partial x_i} + 2\frac{\partial^2 \overline{Y_I}}{\partial \zeta \partial \alpha} \frac{\partial Z}{\partial x_i} \frac{\partial a}{\partial x_i} \\
&\quad + 2\frac{\partial^2 \overline{Y_I}}{\partial x_i \partial \zeta} \frac{\partial Z}{\partial x_i} + 2\frac{\partial^2 \overline{Y_I}}{\partial x_i \partial \alpha} \frac{\partial a}{\partial x_i} + \frac{\partial \overline{Y_I}}{\partial \zeta} \frac{\partial^2 Z}{\partial x_i \partial x_i} \\
&\quad + \frac{\partial \overline{Y_I}}{\partial \alpha} \frac{\partial^2 a}{\partial x_i \partial x_i} + \frac{\partial^2 \overline{Y_I}}{\partial x_i \partial x_i} + \frac{\partial^2 Y_I'}{\partial x_i \partial x_i}.
\end{aligned} \tag{3.6}
$$

Equations (3.4), (3.5), and (3.6) were substituted in Eq. (3.3) producing,

$$
\begin{aligned}
\frac{\dot\omega_I}{\rho} &= E_{\overline{Y_I}} + \frac{\partial \overline{Y_I}}{\partial \zeta} E_Z + \frac{\partial \overline{Y_I}}{\partial \alpha} E_a - D\frac{\partial^2 \overline{Y_I}}{\partial \zeta^2} \frac{\partial Z}{\partial x_i} \frac{\partial Z}{\partial x_i} - D\frac{\partial^2 \overline{Y_I}}{\partial \alpha^2} \frac{\partial a}{\partial x_i} \frac{\partial a}{\partial x_i} \\
&\quad - 2D\frac{\partial^2 \overline{Y_I}}{\partial \zeta \partial \alpha} \frac{\partial Z}{\partial x_i} \frac{\partial a}{\partial x_i} - 2D\frac{\partial^2 \overline{Y_I}}{\partial x_i \partial \zeta} \frac{\partial Z}{\partial x_i} - 2D\frac{\partial^2 \overline{Y_I}}{\partial x_i \partial \alpha} \frac{\partial a}{\partial x_i} + E_{Y_I'}.
\end{aligned} \tag{3.7}
$$

where the following definitions are used:

- The transport equation of the conditional average of the species mass fraction is

$$
E_{\overline{Y_I}} = \frac{\partial \overline{Y_I}}{\partial t} + u_i \frac{\partial \overline{Y_I}}{\partial x_i} - D\frac{\partial^2 \overline{Y_I}}{\partial x_i \partial x_i}. \tag{3.8}
$$

- The transport equation of mixture fraction, Eq. (2.1), is written here as

$$
E_Z = \frac{\partial Z}{\partial t} + u_i \frac{\partial Z}{\partial x_i} - D\frac{\partial^2 Z}{\partial x_i \partial x_i} = 0. \tag{3.9}
$$

- The transport equation of the scalar a is

$$
E_a = \frac{\partial a}{\partial t} + u_i \frac{\partial a}{\partial x_i} - D\frac{\partial^2 a}{\partial x_i \partial x_i} = 0. \tag{3.10}
$$

- The transport equation of the fluctuations around the conditional average of species mass fraction is

$$
E_{Y_I'} = \frac{\partial Y_I'}{\partial t} + u_i \frac{\partial Y_I'}{\partial x_i} - D\frac{\partial^2 Y_I'}{\partial x_i \partial x_i}. \tag{3.11}
$$

3.3 Modelling Scalar Dissipation

Scalar dissipation, $\chi_z = \frac{\partial Z}{\partial x_i} \frac{\partial Z}{\partial x_i}$, is used to represent the coupling that exists between fluid dynamics and the chemical reactions taking place in a turbulent reacting flow [23]. Previous research [1] indicated that large values of scalar dissipation rates lead to extinction of flames. Conversely, ignition phenomena are associated to small scalar dissipation rates.

Peters [1] proposed a model in which the scalar dissipation rate diminished as a function of mixture fraction with time in a one-dimensional mixing layer. This model is frequently used in the flamelet formulation discussed in section 2.6.4. However, the model is not capable of capturing extinction or ignition. An improvement to better reproduce extinction phenomena was proposed by Peters [1] in which a conditional stoichiometric scalar dissipation rate, assumed to have a lognormal PDF, was used to calculate the right proportion of burning flamelets during an extinction event.

Using CMC and the stretched diffusion concept, Bushe [16] proposed a model for the conditional scalar dissipation rate, which was found to provide good approximations of values of the scalar dissipation rate when compared to DNS of a non-reactive flow of Eswaran and Pope [65]. This same model, however, did not provide good estimations of ignition due to long decreasing times of the scalar dissipation [16]. An improvement of this model was to incorporate a second conditioning variable to the system of transport equations of species mass fractions, which was also a passive scalar. This model was found to provide good predictions of ignition and double-flame formation of an n-Heptane non-premixed flame when compared to data obtained by other researchers [66], [67], [68]. However, this formulation did not predict the presence of triple flames found in other research papers [67].

In this thesis, the DCMC method has been applied to define conditionally averaged transport equations for the scalar dissipation of Z and a. The conditional average of scalar dissipation is defined as

$$\overline{\chi_z} = \overline{\chi_z}(\zeta, \alpha; x_i, t) \equiv \langle \chi_z(x_i, t) | Z(x_i, t) = \zeta, a(x_i, t) = \alpha \rangle$$

leading to an instantaneous value of

$$\chi_z(x_k, t) = \overline{\chi_z|_{\zeta = Z(x_i, t), \alpha = a(x_i, t)}} + \chi_z'. \tag{3.12}$$

Ruetsch and Maxey [69] proposed a transport equation for the scalar dissipation, with the terms on the rhs of the equation representing production, dissipation, and diffusion:

$$\frac{D\chi_z}{Dt} = -2 \frac{\partial Z}{\partial x_i} \frac{\partial Z}{\partial x_j} S_{ij} - 2D \left[\frac{\partial}{\partial x_j} \left(\frac{\partial Z}{\partial x_i} \right) \right]^2 + D \frac{\partial^2 \chi_z}{\partial x_j \partial x_j}. \tag{3.13}$$

The S_{ij} term in Eq. (3.13) corresponds to the strain tensor that denotes the production of scalar dissipation through vortex stretching mechanisms. In premixed, turbulent reacting

flows, strain is known to have a strong effect over the stretch history of the flame, which consequently affects the flame structure [11]. The definition of S_{ij} [14] is,

$$S_{ij} = \frac{1}{2}\left(\frac{\partial u_i}{\partial x_j} + \frac{\partial u_j}{\partial x_i}\right),$$ (3.14)

In turbulent, non-premixed flames, high levels of strain imply high levels of scalar dissipation, which in turn generate local extinction of the flame, since the chemical reactions cannot take place given the extremely high rate at which reactants are diffused into and through the reaction zone. Williams [11] provided a flamelet-based analysis of this phenomenon. Thévenin and Candel [67] studied the effect of variable strain on the ignition of a non-premixed flow of air and hydrogen through the use of computer simulations. While their research predicted self-ignition and ignition times in agreement with the experimental results of Cheng et al [70], the triple-flame phenomenon was observed only for the case where there was no strain present.

Using the definition of a material derivative, Eq. (3.13) can be expanded to obtain

$$\frac{\partial \chi_z}{\partial t} = -u_i \frac{\partial \chi_z}{\partial x_j} - 2\frac{\partial Z}{\partial x_i}\frac{\partial Z}{\partial x_j}S_{ij} + D\frac{\partial^2 \chi_z}{\partial x_j \partial x_j} - 2D\left[\left(\frac{\partial^2 Z}{\partial x_j \partial x_i}\right)\left(\frac{\partial^2 Z}{\partial x_j \partial x_i}\right)\right].$$ (3.15)

In order to express Eq. (3.15) in terms of the conditioning variables, it is required to obtain derivatives analogues to Eqs. (3.4), (3.5), and (3.6). The definitions of Eqs. (3.9) and (3.10) are also used to produce

$$\begin{aligned}
\frac{\partial \overline{\chi_z}}{\partial t} &= -\frac{\partial \overline{\chi_z}}{\partial \zeta}E_Z - \frac{\partial \overline{\chi_z}}{\partial \alpha}E_a - E_{\overline{\chi_z'}} - u_i\frac{\partial \overline{\chi_z}}{\partial x_i} - 2\frac{\partial Z}{\partial x_i}\frac{\partial Z}{\partial x_j}S_{ij} + D\frac{\partial^2 \overline{\chi_z}}{\partial x_i \partial x_i} \\
&\quad + D\frac{\partial^2 \overline{\chi_z}}{\partial \zeta^2}\frac{\partial Z}{\partial x_i}\frac{\partial Z}{\partial x_i} + D\frac{\partial^2 \overline{\chi_z}}{\partial \alpha^2}\frac{\partial a}{\partial x_i}\frac{\partial a}{\partial x_i} + 2D\frac{\partial^2 \overline{\chi_z}}{\partial \zeta \partial \alpha}\frac{\partial Z}{\partial x_i}\frac{\partial a}{\partial x_i} + 2D\frac{\partial^2 \overline{\chi_z}}{\partial x_i \partial \zeta}\frac{\partial Z}{\partial x_i} \\
&\quad + 2D\frac{\partial^2 \overline{\chi_z}}{\partial x_i \partial \alpha}\frac{\partial a}{\partial x_i} - 2D\left[\left(\frac{\partial^2 Z}{\partial x_j \partial x_i}\right)\left(\frac{\partial^2 Z}{\partial x_j \partial x_i}\right)\right],
\end{aligned}$$ (3.16)

where the transport equation for the conditionally averaged fluctuation of scalar dissipation is

$$E_{\overline{\chi_z'}} = \frac{\partial \overline{\chi_z'}}{\partial t} + u_i\frac{\partial \overline{\chi_z'}}{\partial x_i} - D\frac{\partial^2 \overline{\chi_z'}}{\partial x_i \partial x_i}$$ (3.17)

The conditionally averaged transport equation of the scalar dissipation χ_a follows analogously to Eqs. (3.16) and (3.17).

3.4 Scalar Transport Closure Hypotheses

Equations (3.7) and (3.16) contain unclosed terms for which closure hypotheses are formulated in this thesis. With the following scalar transport hypotheses, some of the terms in those equations are closed:

- Z and a are conserved scalars, hence its lack of a source term as shown in Eqs. (2.1) and (3.10);

- The spatial gradient of a is perpendicular to the spatial gradient of Z to better capture the effects of fluctuations along isosurfaces of mixture fraction.

Using these hypotheses, Eq. (3.7) is reduced to

$$
\frac{\dot{\omega}_I}{\rho} = E_{\overline{Y_I}} - D\frac{\partial^2 \overline{Y_I}}{\partial \zeta^2}\frac{\partial Z}{\partial x_i}\frac{\partial Z}{\partial x_i} - D\frac{\partial^2 \overline{Y_I}}{\partial \alpha^2}\frac{\partial a}{\partial x_i}\frac{\partial a}{\partial x_i}
$$
$$
-2D\frac{\partial^2 \overline{Y_I}}{\partial x_i \partial \zeta}\frac{\partial Z}{\partial x_i} - 2D\frac{\partial^2 \overline{Y_I}}{\partial x_i \partial \alpha}\frac{\partial a}{\partial x_i} + E_{Y_I'}. \tag{3.18}
$$

Eq. (3.16) is also reduced to

$$
\frac{\partial \overline{\chi_z}}{\partial t} = -E_{\overline{\chi_z'}} - u_i\frac{\partial \overline{\chi_z}}{\partial x_i} - 2\frac{\partial Z}{\partial x_i}\frac{\partial Z}{\partial x_j}S_{ij} + D\frac{\partial^2 \overline{\chi_z}}{\partial x_i \partial x_i}
$$
$$
+D\frac{\partial^2 \overline{\chi_z}}{\partial \zeta^2}\frac{\partial Z}{\partial x_i}\frac{\partial Z}{\partial x_i} + D\frac{\partial^2 \overline{\chi_z}}{\partial \alpha^2}\frac{\partial a}{\partial x_i}\frac{\partial a}{\partial x_i} + 2D\frac{\partial^2 \overline{\chi_z}}{\partial x_i \partial \zeta}\frac{\partial Z}{\partial x_i}
$$
$$
+2D\frac{\partial^2 \overline{\chi_z}}{\partial x_i \partial \alpha}\frac{\partial a}{\partial x_i} - 2D\left[\left(\frac{\partial^2 Z}{\partial x_j \partial x_i}\right)\left(\frac{\partial^2 Z}{\partial x_j \partial x_i}\right)\right]. \tag{3.19}
$$

Multiplying Eq.(3.18) by ρ and taking its conditional average yields

$$
\overline{\dot{\omega}}_I = \overline{\rho E_{\overline{Y_I}}} + \overline{\rho E_{Y_I'}} - \frac{\partial^2 \overline{Y_I}}{\partial \zeta^2}\overline{\rho D\frac{\partial Z}{\partial x_i}\frac{\partial Z}{\partial x_i}} - \frac{\partial^2 \overline{Y_I}}{\partial \alpha^2}\overline{\rho D\frac{\partial a}{\partial x_i}\frac{\partial a}{\partial x_i}}
$$
$$
-2\frac{\partial^2 \overline{Y_I}}{\partial x_i \partial \zeta}\overline{\rho D\frac{\partial Z}{\partial x_i}} - 2\frac{\partial^2 \overline{Y_I}}{\partial x_i \partial \alpha}\overline{\rho D\frac{\partial a}{\partial x_i}}. \tag{3.20}
$$

Conditionally-averaging Eq. (3.19) yields

$$
\frac{\partial \overline{\chi_z}}{\partial t} = -\overline{E_{\overline{\chi_z'}}} - u_i\overline{\frac{\partial \overline{\chi_z}}{\partial x_i}} - 2\overline{\frac{\partial Z}{\partial x_i}\frac{\partial Z}{\partial x_j}S_{ij}} + D\overline{\frac{\partial^2 \overline{\chi_z}}{\partial x_i \partial x_i}}
$$
$$
+D\frac{\partial^2 \overline{\chi_z}}{\partial \zeta^2}\overline{\frac{\partial Z}{\partial x_i}\frac{\partial Z}{\partial x_i}} + D\frac{\partial^2 \overline{\chi_z}}{\partial \alpha^2}\overline{\frac{\partial a}{\partial x_i}\frac{\partial a}{\partial x_i}} + 2D\frac{\partial^2 \overline{\chi_z}}{\partial x_i \partial \zeta}\overline{\frac{\partial Z}{\partial x_i}}
$$
$$
+2D\frac{\partial^2 \overline{\chi_z}}{\partial x_i \partial \alpha}\overline{\frac{\partial a}{\partial x_i}} - 2D\overline{\left[\left(\frac{\partial^2 Z}{\partial x_j \partial x_i}\right)\left(\frac{\partial^2 Z}{\partial x_j \partial x_i}\right)\right]}. \tag{3.21}
$$

3.5 DCMC Closure Hypotheses

Equations (3.20) and (3.21) were reduced to a conditionally-averaged form in the previous section. Whilst closure was determined for some unclosed terms, both equations still contain terms that can be further closed using the DCMC closure hypotheses described in the following modelling assumptions.

- DCMC Modelling Assumption 1: the fluctuations around the conditional mean of species mass fraction and around the conditional mean of scalar dissipation are only functions of the scalar variables Z and a, independent of time and space. This produces

$$\overline{\rho}\frac{\partial \overline{Y_I'}}{\partial t} + \overline{\rho u_i}\frac{\partial \overline{Y_I'}}{\partial x_i} - \overline{\rho D}\frac{\partial^2 \overline{Y_I'}}{\partial x_i \partial x_i} = 0. \tag{3.22}$$

$$\frac{\partial \overline{\chi_z'}}{\partial t} + \overline{u_i}\frac{\partial \overline{\chi_z'}}{\partial x_i} - \overline{D}\frac{\partial^2 \overline{\chi_z'}}{\partial x_i \partial x_i} = 0. \tag{3.23}$$

- DCMC Modelling Assumption 2: assuming that the flow is homogeneous and isotropic, the ensemble of conditional averages of species mass fractions and scalar dissipation are equal at each point in space for the same instant in time, and the spatial gradient of the conditional mean of the species mass fraction is equal to zero [16]. This yields

$$\overline{\rho u_i}\frac{\partial \overline{Y_I}}{\partial x_i} = 0 \tag{3.24}$$

$$\overline{\rho D}\frac{\partial^2 \overline{Y_I}}{\partial x_i \partial x_i} = 0 \tag{3.25}$$

$$\overline{\frac{\partial^2 \overline{Y_I}}{\partial x_i \partial \zeta} \rho D \frac{\partial Z}{\partial x_i}} = 0 \tag{3.26}$$

$$\overline{\frac{\partial^2 \overline{Y_I}}{\partial x_i \partial \alpha} \rho D \frac{\partial a}{\partial x_i}} = 0 \tag{3.27}$$

$$\overline{u_i \frac{\partial \overline{\chi_z}}{\partial x_i}} = 0 \tag{3.28}$$

$$\overline{D \frac{\partial^2 \overline{\chi_z}}{\partial x_i \partial x_i}} = 0 \tag{3.29}$$

$$\overline{D \frac{\partial^2 \overline{\chi_z}}{\partial x_i \partial \zeta} \frac{\partial Z}{\partial x_i}} = 0 \tag{3.30}$$

$$\overline{D \frac{\partial^2 \overline{\chi_z}}{\partial x_i \partial \alpha} \frac{\partial a}{\partial x_i}} = 0. \tag{3.31}$$

Substituting Eqs. (3.22) and (3.24) - (3.27) in Eq. (3.20) results in

$$\overline{\dot{\omega}_I} = \overline{\rho}\frac{\partial \overline{Y_I}}{\partial t} - \frac{\partial^2 \overline{Y_I}}{\partial \zeta^2}\overline{\rho D \frac{\partial Z}{\partial x_i}\frac{\partial Z}{\partial x_i}} - \frac{\partial^2 \overline{Y_I}}{\partial \alpha^2}\overline{\rho D \frac{\partial a}{\partial x_i}\frac{\partial a}{\partial x_i}}. \tag{3.32}$$

Here, the term on the lhs represents the conditional average of chemical source term, while the second and third terms on the rhs represent the conditional average of diffusion of the species mass fractions in the scalar field.

Substituting Eqs. (3.17) and (3.28) - (3.31) in Eq. (3.21) results in

$$\frac{\partial \overline{\chi_z}}{\partial t} = -2\overline{\frac{\partial Z}{\partial x_i}\frac{\partial Z}{\partial x_j}S_{ij}} + D\frac{\partial^2 \overline{\chi_z}}{\partial \zeta^2}\overline{\chi_z} + D\frac{\partial^2 \overline{\chi_z}}{\partial \alpha^2}\overline{\chi_a} - 2D\overline{\frac{\partial^2 Z}{\partial x_j \partial x_i}\frac{\partial^2 Z}{\partial x_j \partial x_i}}. \qquad (3.33)$$

Here, the first term on the rhs represents the conditional average of production of scalar dissipation, the second and third terms represent the conditional average of diffusion of scalar dissipation, and the third term represents the conditional average of dissipation of scalar dissipation.

3.6 Mathematical solution of the Z-gradient squared term

We define

$$\Phi = \overline{\frac{\partial^2 Z}{\partial x_j \partial x_i}\frac{\partial^2 Z}{\partial x_j \partial x_i}} \qquad (3.34)$$

$$\Theta = \overline{\frac{\partial \chi_z}{\partial x_j}\frac{\partial \chi_z}{\partial x_j}}. \qquad (3.35)$$

Expanding Θ yields,

$$\frac{\partial \chi_z}{\partial x_j}\frac{\partial \chi_z}{\partial x_j} = \left(\frac{\partial \chi_z}{\partial x_j}\right)^2$$

$$\left(\frac{\partial \chi_z}{\partial x_j}\right)^2 = \left[\frac{\partial}{\partial x_j}\left(\frac{\partial Z}{\partial x_i}\frac{\partial Z}{\partial x_i}\right)\right]^2$$

$$\left[\frac{\partial}{\partial x_j}\left(\frac{\partial Z}{\partial x_i}\frac{\partial Z}{\partial x_i}\right)\right]^2 = \left[2\frac{\partial^2 Z}{\partial x_j \partial x_i}\frac{\partial Z}{\partial x_i}\right]^2$$

$$\left[2\frac{\partial^2 Z}{\partial x_j \partial x_i}\frac{\partial Z}{\partial x_i}\right]^2 = 4\left(\frac{\partial^2 Z}{\partial x_j \partial x_i}\frac{\partial^2 Z}{\partial x_j \partial x_i}\right)\left(\frac{\partial Z}{\partial x_i}\frac{\partial Z}{\partial x_i}\right) \qquad (3.36)$$

Comparing Eq. (3.36) to Eq. (3.34) it can be seen that

$$\Theta = 4\Phi\chi_z, \text{and}$$

$$\Phi = \frac{1}{4\chi_z}\Theta. \qquad (3.37)$$

Using Eq. (3.12) and taking partial derivatives of χ_z with respect to space, Eq. (3.35) can be expressed as

$$
\begin{aligned}
\Theta = {} & \left(\frac{\partial \overline{\chi_z}}{\partial x_j}\right)^2 + \left(\frac{\partial \overline{\chi_z}}{\partial \zeta}\frac{\partial Z}{\partial x_j}\right)^2 + \left(\frac{\partial \overline{\chi_z}}{\partial \alpha}\frac{\partial a}{\partial x_j}\right)^2 + \left(\frac{\partial \chi_z'}{\partial x_j}\right)^2 \\
& + 2\frac{\partial \overline{\chi_z}}{\partial x_j}\frac{\partial \overline{\chi_z}}{\partial \zeta}\frac{\partial Z}{\partial x_j} + 2\frac{\partial \overline{\chi_z}}{\partial x_i}\frac{\partial \overline{\chi_z}}{\partial \alpha}\frac{\partial a}{\partial x_j} + 2\frac{\partial \overline{\chi_z}}{\partial \zeta}\frac{\partial Z}{\partial x_j}\frac{\partial \overline{\chi_z}}{\partial \alpha}\frac{\partial a}{\partial x_j} \\
& + 2\frac{\partial \overline{\chi_z}}{\partial x_j}\frac{\partial \chi_z'}{\partial x_j} + 2\frac{\partial \overline{\chi_z}}{\partial \zeta}\frac{\partial Z}{\partial x_j}\frac{\partial \chi_z'}{\partial x_j} + 2\frac{\partial \overline{\chi_z}}{\partial \alpha}\frac{\partial a}{\partial x_j}\frac{\partial \chi_z'}{\partial x_j}.
\end{aligned}
\tag{3.38}
$$

Using the scalar transport closure hypotheses and the modelling assumptions, Eq. (3.38) reduces to

$$
\Theta = \left(\frac{\partial \overline{\chi_z}}{\partial \zeta}\right)^2 \chi_z + \left(\frac{\partial \overline{\chi_z}}{\partial \alpha}\right)^2 \chi_a.
\tag{3.39}
$$

Substituting Eq. (3.39) in Eq. (3.37) and conditionally-averaging, yields

$$
\overline{\Phi} = \frac{1}{4}\left(\frac{\partial \overline{\chi_z}}{\partial \zeta}\right)^2 + \frac{1}{4}\left(\frac{\partial \overline{\chi_z}}{\partial \alpha}\right)^2 \overline{\left(\frac{\chi_a}{\chi_z}\right)}.
\tag{3.40}
$$

It is further assumed that

$$
\overline{\left(\frac{\chi_a}{\chi_z}\right)} = \frac{\overline{\chi_a}}{\overline{\chi_z}}.
\tag{3.41}
$$

Using this assumption in Eq. (3.40) and substituting this result in Eq. (3.33) produces the final version of the conditionally-averaged transport equation of scalar dissipation of mixture fraction and of the scalar a

$$
\begin{aligned}
\frac{\partial \overline{\chi_z}}{\partial t} = {} & -2\overline{\frac{\partial Z}{\partial x_i}\frac{\partial Z}{\partial x_j}S_{ij}} - \frac{D}{2}\left(\frac{\partial \overline{\chi_z}}{\partial \zeta}\right)^2 - \frac{D}{2}\left(\frac{\partial \overline{\chi_z}}{\partial \alpha}\right)^2 \frac{\overline{\chi_a}}{\overline{\chi_z}} \\
& + D\frac{\partial^2 \overline{\chi_z}}{\partial \zeta^2}\overline{\chi_z} + D\frac{\partial^2 \overline{\chi_z}}{\partial \alpha^2}\overline{\chi_a}
\end{aligned}
\tag{3.42}
$$

$$
\begin{aligned}
\frac{\partial \overline{\chi_a}}{\partial t} = {} & -2\overline{\frac{\partial a}{\partial x_i}\frac{\partial a}{\partial x_j}S_{ij}} - \frac{D}{2}\left(\frac{\partial \overline{\chi_a}}{\partial \zeta}\right)^2 - \frac{D}{2}\left(\frac{\partial \overline{\chi_a}}{\partial \alpha}\right)^2 \frac{\overline{\chi_z}}{\overline{\chi_a}} \\
& + D\frac{\partial^2 \overline{\chi_a}}{\partial \zeta^2}\overline{\chi_z} + D\frac{\partial^2 \overline{\chi_a}}{\partial \alpha^2}\overline{\chi_a}.
\end{aligned}
\tag{3.43}
$$

The first term on the rhs of these transport equations describes the conditional average of production of scalar dissipation. This term represents the mapping of the strain tensor S_{ij} onto the corresponding diffusing scalar's surface. The second and third terms represent the conditional average of dissipation of scalar dissipation, while the last two terms represent the conditional average of diffusion of scalar dissipation. All the terms in these equations are closed, with the exception of the term containing the strain tensor S_{ij}, which has to be modelled.

3.7 Models for the Transport Equation of Scalar Dissipation

Two different models using stochastic processes are proposed to model the strain tensor S_{ij}. The first model uses a periodic force with random phase shifting to simulate the chaotic behaviour of the strain tensor. A second model uses the Coupled Map Lattices (CML) developed by Beck and Hilgers [5], [6], [7] to simulate velocity increments in an isotropic, homogeneous, fully-developed turbulent flow, from which the corresponding strain tensor is calculated.

Pitsch and Fedotov [71] simulated the fluctuations of the scalar dissipation rate in non-premixed combustion. They used this approach in combination with a flamelet formulation to simulate a turbulent, non-premixed reactive flow of methane and air. They reported that the extinction process occured at smaller time scales than those relevant to the overall phenomenon, like turbulent or chemical time scales. This seems to indicate that the deviations are due to Gaussian white noise, resulting in a Wiener process. This research group also found delimiting regimes that drive the burning and extinguishing states and that even small-amplitude scalar dissipation fluctuations have considerable effects on the state of the flame, taking it from the burning to the extinguished state. This finding in particular, further reinforced the need to study the influence of the scalar dissipation rate on a turbulent, non-premixed reacting flow, which is one objective of this thesis.

3.7.1 Periodic Forcing with Random Phase Shifting (PF)

The use of forcing schemes involving harmonic functions has been explored in DNS simulations of isotropic, homogeneous turbulence [72], [73]. The general idea behind this method is to generate an influx of energy at low Fourier wavenumbers that compensates for the dissipative effects at the small scales of turbulence.

Eswaran and Pope [73], used a stochastic forcing scheme with an Ornstein-Uhlenbeck formulation to study the validity and capabilities of the method in an isotropic, homogeneous turbulent flow. Hilgers et al [74] explored the use of stochastic resonance to the study of motion of an overdamped particle in a bistable potential, subject to a external periodic perturbations and coloured noise.

Similar to the work by Eswaran and Pope [73], the first model proposed in this thesis uses a combination of harmonic signals to mimic the chaotic influence of the turbulent flow field on the strain tensor by using the product of the signals in the x and y directions:

$$\Psi_n = A_n \sin\left(\omega_{nx} x + \theta_{nx}\right) \sin\left(\omega_{ny} y + \theta_{ny}\right). \tag{3.44}$$

Here,

- The magnitude of the amplitudes is $A_{n+1} = A_n/2$, and is scaled by the Reynolds number of the flow.

- The period of the signals is $\omega_{n+1} = 2\omega_n$ and is used as an emulator of the viscosity of the flow. Larger periodicity implies a higher number of transitions, which are interpreted as lower viscosity.

- The random phase shift θ_n is produced with Gaussian random numbers. This shifting is used to produce random fluctuations in the strain field.

- $n = 1...N$ is the number of signals that are then combined to obtain the assumed strain tensor field in the $x - y$ space:

$$S_{ij}(x, y) = \sum_{i=1}^{n} \Psi_n. \tag{3.45}$$

The coupling between the strain field and the flow is obtained by forcing proportionality between the amplitudes A_n of the signals and the magnitude of the characteristic Reynolds number of the flow. This implies that this scheme can only simulate strain fields for one energy level at a time and must be calibrated for each energy level independently. For decaying, isotropic, homogeneous, turbulence, characteristic parameters can be used to scale the magnitude of the strain field accordingly with turbulence theory [14] as,

$$|S_{ij}| = \sqrt{\frac{\epsilon}{2\nu}}. \tag{3.46}$$

The structure of the strain fields simulated with the PF model can be modified by varying the number of signals used in the calculation of Eq. (3.45), by varying the scaling of the amplitudes between signals, or by varying the periodicity of Eq. (3.44).

The PF scheme was used in this thesis to simulate strain fields with fluctuations and magnitudes relevant to the combustion process studied. The magnitudes were compared to

those obtained from the DNS of Bushe [8] and the simulated fields in the $x - y$ space were then transformed to the $\alpha - \zeta$ space using a simple mapping convention. The mapping is performed by assuming a linear correspondence between α and x, and $\zeta = \mathrm{erf}(y)$.

3.7.2 Coupled Map Lattices (CML)

The second model that has been implemented uses the turbulent flow simulation proposed in the works by Beck [5] and Hilgers and Beck [6], [7]. This model is a coupled map lattice that mimics the energy cascade in a turbulent flow. The system of equations is as follows

$$
\begin{aligned}
x_{d,n}(i) &= F(x_{d,n-1}(i)) \\
u_{d,n}^{(1)}(i) &= \lambda_1 u_{d,n-1}^{(1)}(i) + \frac{g}{2D}\left(\sum_\sigma u_{d,n-1}^{(1)}(i+\sigma)\right) + x_{d,n}(i) \\
u_{d,n}^{(k)}(i) &= \lambda_k u_{d,n-1}^{(k)}(i) + \frac{g}{2D}\left(\sum_\sigma u_{d,n-1}^{(k)}(i+\sigma)\right) \\
&\quad + C\zeta_{d,n-1}^{(k-1)}(i)(1-\lambda_{k-1})u_{d,n-1}^{(k-1)}(i).
\end{aligned}
\tag{3.47}
$$

In this model,

- $F(x)$ is a map that models the energy input from the large scales and is defined as $F(x) = 1 - 2x^2$, where x is the position of stochastic particles in D spatial dimensions.

- The parameter k corresponds to the energy level in the cascade. High-values of k imply higher energy-dissipation processes, which leads to a lower energy level.

- The coupling parameter g is associated with, and should be scaled to, the molecular viscosity, μ, of the fluid.

- The damping parameter λ is defined as $\lambda = exp(-\gamma\tau k)$, where the product $\gamma\tau$ is proportional to the inverse Reynolds number.

- The product $C\zeta$ is used to determine the random fraction of the driving momentum that each of the 'daughter' eddies receive from the previous higher scale.

The calculated temporal velocity difference u is later used to calculate the strain rate tensor using Eq. (3.46), or, under the assumption of decaying, isotropic, homogeneous turbulence, it can be further demonstrated [14] that,

$$
S_{ij} = \sqrt{\frac{15}{2}\left(\frac{\partial u_i}{\partial x_j}\right)^2}.
\tag{3.48}
$$

Using the CML model, the strain fields were simulated in the $x - y$ plane and later mapped onto the $\alpha - \zeta$ plane using the same mapping convention as used in the PF model: $(\alpha, \zeta) \rightarrow (x, \text{erf}(y))$.

It is clear that while this model is capable of simulating strain fields for a wide range of energy levels, the main focus of this research is on the simulation of strain fields at the energy levels relevant to the combustion process studied. This means that the CML had to be capable of simulating velocity increment fields at relatively small scales. This calibration was made possible by using the variable k that denotes the energy level at which the velocity fields are calculated. The target value of k was obtained by running a number of simulations and comparing the results with statistics from the DNS of Bushe et al [8]. A consequence of this is that all the previous energy levels still have to be calculated, which inevitably increased the computation time.

3.8 Summary

The DCMC equations that describe turbulent combustion events using two conditioning variables have been derived in this chapter, resulting in the following system of equations

$$
\begin{aligned}
\bar{\omega}_I &= \overline{\rho \frac{\partial Y_I}{\partial t}} - \overline{\frac{\partial^2 Y_I}{\partial \zeta^2} \rho D \frac{\partial Z}{\partial x_i} \frac{\partial Z}{\partial x_i}} - \overline{\frac{\partial^2 Y_I}{\partial \alpha^2} \rho D \frac{\partial a}{\partial x_i} \frac{\partial a}{\partial x_i}} \\
\frac{\partial \overline{\chi_z}}{\partial t} &= -2 \overline{\frac{\partial Z}{\partial x_i} \frac{\partial Z}{\partial x_j} S_{ij}} - \frac{D}{2} \left(\frac{\partial \overline{\chi_z}}{\partial \zeta} \right)^2 - \frac{D}{2} \left(\frac{\partial \overline{\chi_z}}{\partial \alpha} \right)^2 \frac{\overline{\chi_a}}{\overline{\chi_z}} \\
&\quad + D \frac{\partial^2 \overline{\chi_z}}{\partial \zeta^2} \overline{\chi_z} + D \frac{\partial^2 \overline{\chi_z}}{\partial \alpha^2} \overline{\chi_a} \\
\frac{\partial \overline{\chi_a}}{\partial t} &= -2 \overline{\frac{\partial a}{\partial x_i} \frac{\partial a}{\partial x_j} S_{ij}} - \frac{D}{2} \left(\frac{\partial \overline{\chi_a}}{\partial \zeta} \right)^2 - \frac{D}{2} \left(\frac{\partial \overline{\chi_a}}{\partial \alpha} \right)^2 \frac{\overline{\chi_z}}{\overline{\chi_a}} \\
&\quad + D \frac{\partial^2 \overline{\chi_a}}{\partial \zeta^2} \overline{\chi_z} + D \frac{\partial^2 \overline{\chi_a}}{\partial \alpha^2} \overline{\chi_a}.
\end{aligned}
\tag{3.49}
$$

The properties and characteristics of the second conditional variable a have also been described and applied during the derivation of the equations. In this chapter, closure for the DCMC equations has been proposed using scalar transport and CMC closure hypotheses. The resulting equation contains a strain rate tensor term that has been modelled using two different stochastic processes. The results obtained from the use of these models are presented in the following chapter.

Chapter 4

Simulation of Methane Oxidation with DCMC-SP

The system of equations developed in the previous chapter, Eq. (3.49), is used to simulate the combustion of methane and air. The present chapter describes the results obtained from this computational simulation. The chemical kinetic mechanism, as well as the initial and boundary conditions developed for the generation of both the DNS and CMC databases have been used in this research. The DNS database has also been used as a source of information for the evolution of the turbulent flow. This means that the results presented in this thesis have been produced in an *a priori* sense. A comparison between the DCMC-SP results of this thesis and the CMC [9] and DNS [8] for a similar test case shows that the DCMC-SP implementation offers an improvement over the singly-conditional moment closure method.

4.1   The Reference DNS and CMC Databases

The DNS database of Bushe et al [8] described the results of a number of independent runs of a shear-free, decaying, turbulent mixing layer. A CMC simulation of the same test case [9] provided good predictions of temperature and mass fractions of the major species while falling short of providing good predictions of *NO* and intermediate mass fractions.

4.1.1   Flow Field

The flow field simulated in the DNS database is a three-dimensional shear-free, temporal mixing layer, discretised by a 240 × 120 × 120 grid, in which the governing equations for incompressible flow were resolved. The domain is periodic in two directions, while allowing outflow in the third direction. The domain is shown in Fig. 4.1. Here, region A denotes the approximate spatial domain where the mixing between fuel and oxidiser occurs.
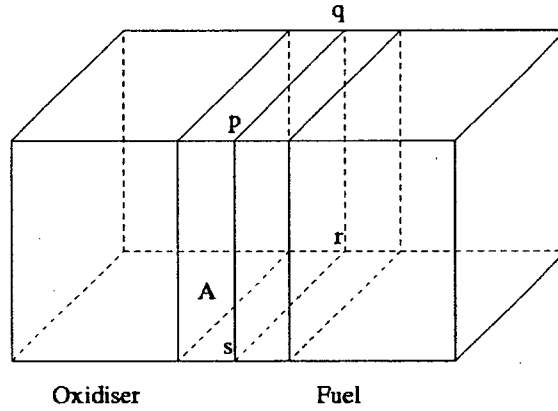
Figure 4.1: DNS computational domain

The initial turbulent flow field was forced using the pseudo-spectral scheme of Ruetsch and Maxey [69] that simulates a statistically stationary, incompressible turbulent flow. The initial Taylor Reynolds number was 59 and the Prandtl and Schmidt numbers used were both set to a constant value of 0.75.

4.1.2 Chemical Kinetics

The chemical kinetic mechanism developed for the DNS database [8] has been used in this research project to determine the effectiveness of the model proposed in Chapter 3. This mechanism involves three steps and is a modification of the two-step reduced mechanism originally proposed by Williams [75], and later modified by Swaminathan and Bilger [76] for the oxidation of methane, with the addition of a third step for NO formation with the Zel'dovich mechanism. The resulting three-step mechanism is written here as

$$F + Oxi \rightarrow I + P$$

$$I + Oxi \rightarrow 2P$$

$$N_2 + Oxi \rightarrow 2NO$$
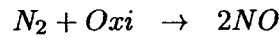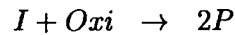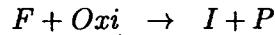
where F is CH_4, Oxi is O_2, and

$$I = \left(\frac{4}{3}H_2 + \frac{2}{3}CO\right)$$

$$P = \left(\frac{2}{3}H_2O + \frac{1}{3}CO_2\right).$$

An important feature of this mechanism is the presence of a steady-state approximation for the mass fraction of the Hydrogen radical. This expression has been designed to emulate the

reduction in the concentration of the Hydrogen radical at low temperatures. The mechanism was further simplified by Bushe et al [8] by assuming peak temperatures in the 1200-2230 K range, so that the computational expense is reduced, while keeping acceptable levels of accuracy. The mechanism was non-dimensionalised by assuming that the constant pressure specific heat C_p, the ratio of specific heats γ, and the speed of sound c remain constant. It was also found that the region where the chemical reaction takes place needed to be broadened to avoid the computational expense associated with the calculation of sharp gradients.

4.1.3 Initial Conditions

Since the chemical kinetic mechanism used in the DNS is not capable of auto-ignition, the initial conditions of the scalars were taken from a planar, laminar flame, which also served as the initial conditions for the CMC simulations. The initial conditions as a function of mixture fraction are shown in Fig. 4.2. This laminar flame was located in the plane formed by points $pqrs$ in Fig. 4.1.
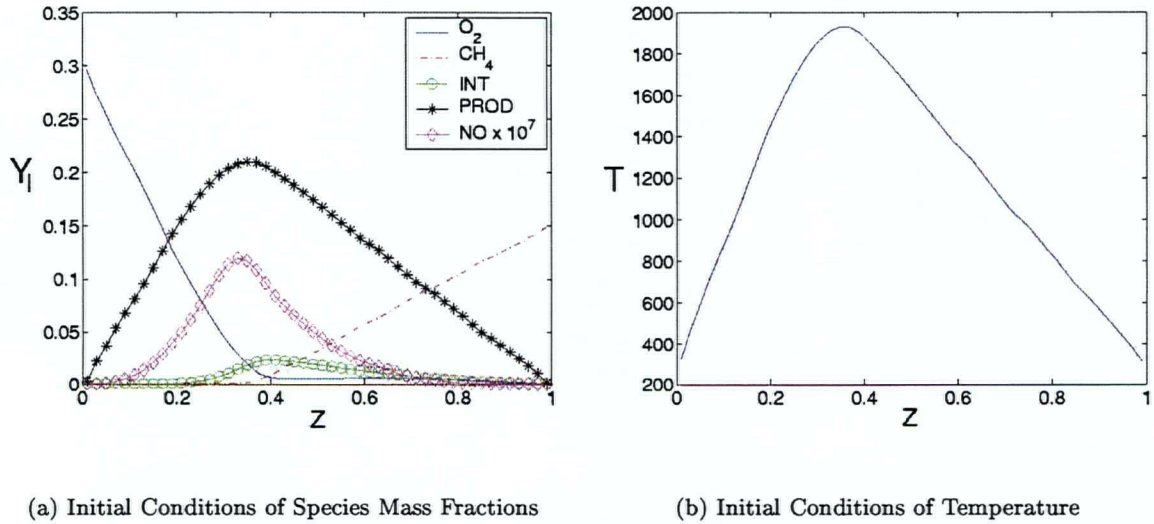

(a) Initial Conditions of Species Mass Fractions

(b) Initial Conditions of Temperature

Figure 4.2: Initial Conditions of the Scalar Fields

4.2 Simulation of CH_4 Oxidation Using DCMC-SP

Using the chemical kinetic mechanism described in the previous section, Eq. (3.49) is expanded to include the species present in the chemical kinetics mechanism, as well as the conditioning

scalar variables, resulting in the following system of equations

$$
\bar{\rho}\frac{\partial \overline{Y}_{O_2}}{\partial t} = \bar{\omega}_{O_2} + \frac{\partial^2 \overline{Y}_{O_2}}{\partial \zeta^2}\rho D\overline{\chi_z} + \frac{\partial^2 \overline{Y}_{O_2}}{\partial \alpha^2}\rho D\overline{\chi_a}
$$

$$
\bar{\rho}\frac{\partial \overline{Y}_{F}}{\partial t} = \bar{\omega}_{F} + \frac{\partial^2 \overline{Y}_{F}}{\partial \zeta^2}\rho D\overline{\chi_z} + \frac{\partial^2 \overline{Y}_{F}}{\partial \alpha^2}\rho D\overline{\chi_a}
$$

$$
\bar{\rho}\frac{\partial \overline{Y}_{I}}{\partial t} = \bar{\omega}_{I} + \frac{\partial^2 \overline{Y}_{I}}{\partial \zeta^2}\rho D\overline{\chi_z} + \frac{\partial^2 \overline{Y}_{I}}{\partial \alpha^2}\rho D\overline{\chi_a}
$$

$$
\bar{\rho}\frac{\partial \overline{Y}_{P}}{\partial t} = \bar{\omega}_{P} + \frac{\partial^2 \overline{Y}_{P}}{\partial \zeta^2}\rho D\overline{\chi_z} + \frac{\partial^2 \overline{Y}_{P}}{\partial \alpha^2}\rho D\overline{\chi_a}
$$

$$
\bar{\rho}\frac{\partial \overline{Y}_{NO}}{\partial t} = \bar{\omega}_{NO} + \frac{\partial^2 \overline{Y}_{NO}}{\partial \zeta^2}\rho D\overline{\chi_z} + \frac{\partial^2 \overline{Y}_{NO}}{\partial \alpha^2}\rho D\overline{\chi_a}
$$

$$
\bar{\rho}\frac{\partial \overline{T}}{\partial t} = \bar{\omega}_{T} + \frac{\partial^2 \overline{T}}{\partial \zeta^2}\rho D\overline{\chi_z} + \frac{\partial^2 \overline{T}}{\partial \alpha^2}\rho D\overline{\chi_a}
$$

$$
\frac{\partial \overline{\chi_a}}{\partial t} = -2\overline{\frac{\partial a}{\partial x_i}\frac{\partial a}{\partial x_j}S_{ij}} - \frac{D}{2}\left(\frac{\partial \overline{\chi_a}}{\partial \zeta}\right)^2 - \frac{D}{2}\left(\frac{\partial \overline{\chi_a}}{\partial \alpha}\right)^2\frac{\overline{\chi_z}}{\overline{\chi_a}}
$$
$$
+ D\frac{\partial^2 \overline{\chi_a}}{\partial \zeta^2}\overline{\chi_z} + D\frac{\partial^2 \overline{\chi_a}}{\partial \alpha^2}\overline{\chi_a}
$$

$$
\frac{\partial \overline{\chi_z}}{\partial t} = -2\overline{\frac{\partial Z}{\partial x_i}\frac{\partial Z}{\partial x_j}S_{ij}} - \frac{D}{2}\left(\frac{\partial \overline{\chi_z}}{\partial \zeta}\right)^2 - \frac{D}{2}\left(\frac{\partial \overline{\chi_z}}{\partial \alpha}\right)^2\frac{\overline{\chi_a}}{\overline{\chi_z}}
$$
$$
+ D\frac{\partial^2 \overline{\chi_z}}{\partial \zeta^2}\overline{\chi_z} + D\frac{\partial^2 \overline{\chi_z}}{\partial \alpha^2}\overline{\chi_a}. \tag{4.1}
$$

This system of equations was solved for a 50×50, $\alpha - \zeta$ grid, with the initial calculation of the strain fields in the $x - y$ space and later mapped onto the $\alpha - \zeta$ space using the simple mapping convention described in Sections 3.7.1 and 3.7.2. The boundary conditions for the strain fields were set to be periodic for both directions. The boundary conditions for all the reacting scalars were set to be periodic in the direction of α and constant in the direction of ζ. The initial conditions of the reacting scalars and of scalar dissipation of mixture fraction were taken directly from the laminar flame described in Section 4.1.3.

The results obtained from the numerical implementation of the system in Eq. (4.1) are presented in this section. Once the strain field was simulated using either of the stochastic processes, the ODE solver DVODE [77] was used to solve Eq. (4.1). Fig. 4.3 serves as an illustration of the structure of the code.
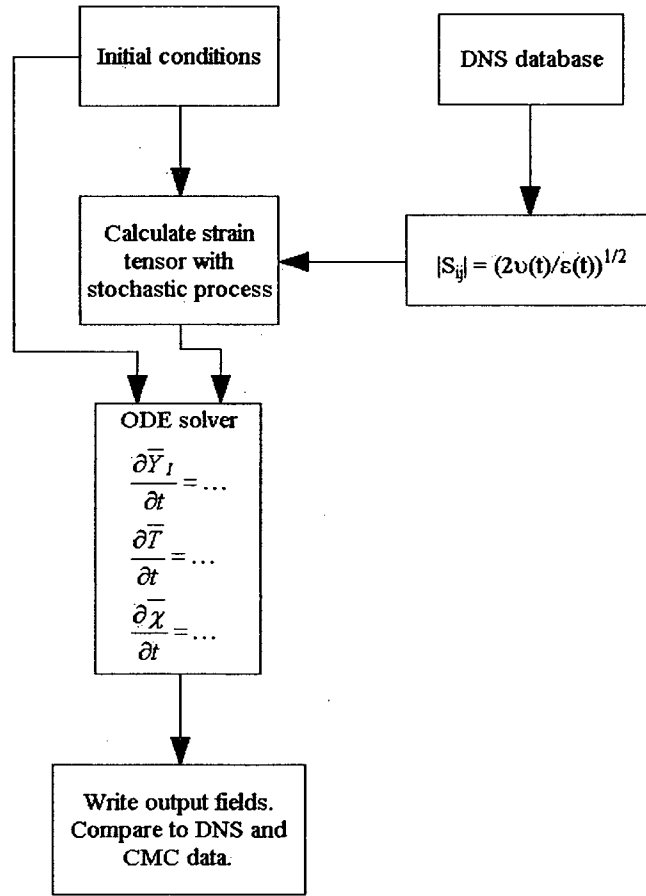
Figure 4.3: DCMC-SP code structure

4.2.1 Simulation of the Strain Field

As discussed in Chapter 3, the strain field has been simulated using two different stochastic processes. This section summarises the results obtained for both cases. Unless expressed otherwise, the figures in this section show results obtained after a calculation time of $t = 5$ time units. In this computational implementation, the following model has been used:

$$-2\overline{\frac{\partial Z}{\partial x_i}\frac{\partial Z}{\partial x_j}}S_{ij} = -2\overline{\chi_Z n_i n_j S_{ij}} \approx -2\overline{\chi_Z}\overline{n_i n_j S_{ij}}.$$

Where n_i and n_j are unity vectors in the direction of the x_i and x_j directions of the gradients of Z. The value of $n_i n_j$ is then $[-1 + 1]$. Bushe and Cant [78] showed that positive values of $n_i n_j$ are statistically more frequent; as a result, it is assumed in this research that $n_i n_j$ is negative if the strain S_{ij} is negative and positive otherwise. This model applies analogously to the corresponding term in the transport equation of χ_a.

Periodic Forcing with Random Phase Shifting (PF)

This model was validated using the stochastic variables $X(x, y; t)$ and $Y(x, y; t)$ in the solution of Eqs. (3.44) and (3.45).

Using statistics from the DNS database of Bushe et al [8], it was found that the appropriate values to simulate a strain field with similar characteristics using the PF model were,

- $A_1 = 1.585$ this parameter is proportional to the Taylor Reynolds number of the DNS database

- $\omega_{1x} = \omega_{1y} = 2\pi$ which indicates the periodicity of the signals. This parameter was set empirically by comparing the structure of the strain fields from the DNS database and the strain fields obtained using the PF model.

The magnitude of the strain tensor was calculated using the values of the parameters ϵ and ν from the DNS database. In all cases, the strain field was first calculated in the $x - y$ plane and later transformed to the $\alpha - \zeta$ plane following the mapping rules described in Section 3.6.

Figure 4.4(a) shows the results of the calculation of the strain field in the $x - y$ plane using $\Psi = 3$ periodic signals. Figure 4.4(b) shows the same strain field after being transformed to the $\alpha - \zeta$ plane. Comparing Figs. 4.4(a) and 4.4(b) it can be seen that the main effect of the coordinate transformation is an apparent *reduction of the area of influence* of the structures close to mixture fraction values of 0 and 1, followed by an *elongation of the area of influence* of those structures between the aforementioned regions of Z.

These two figures also show that the overall magnitudes of the strain field are maintained, while the *reduction - elongation - reduction* effect makes some of the structures disappear, especially for regions in the vicinity of $Z = 0$. This finding is of relevance since the areas where the *elongation* effect is prevalent, is where values of mixture fraction indicate a more vigorous mixing process, where chemical processes are taking place with more frequency. As expected, the *reduction - elongation - reduction* effect does not take place along the α direction. The strain fields are also shown to be periodic in the x, y, α, and ζ directions.

Figures 4.4(c) and 4.4(d), show the strain fields in the $\alpha - \zeta$ space for $\Psi = 4$ and $\Psi = 5$ periodic signals, respectively. From Figs. 4.4(b), 4.4(c), and 4.4(d), it can be seen that the number of signals used has a significant effect on the structure and propagation of the calculated field.
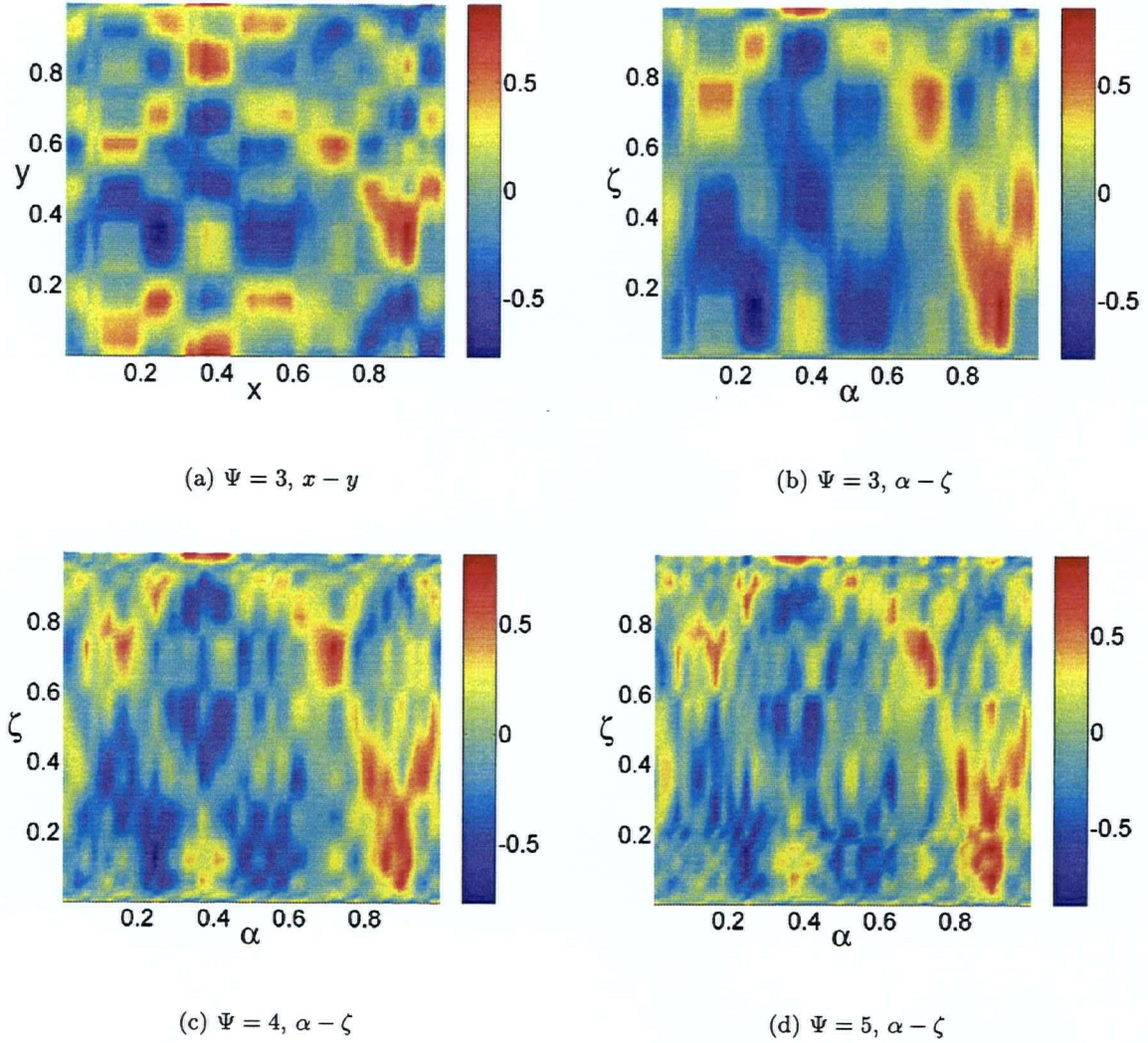

(a) $\Psi = 3$, $x - y$

(b) $\Psi = 3$, $\alpha - \zeta$

(c) $\Psi = 4$, $\alpha - \zeta$

(d) $\Psi = 5$, $\alpha - \zeta$

Figure 4.4: Strain fields simulated with PF

The strain field calculated with three periodic signals shows well-defined regions of positive and negative values of strain, which have the physical meaning of stretch and compression regions in the flow. These structures tend to be very large for this particular case and do not show much intermittency. The structures can be considered to be *eddies*, which implies that large structures correspond to the energy-containing subrange or the inertial subrange

in the cascade model. Consequently, smaller, finer structures would represent the behaviour of a flow at the dissipation subrange, at which combustion is assumed to take place. Figures 4.4(c) and 4.4(d) show a much finer structure with more intermittency than Fig. 4.4(b) while yielding similar strain magnitudes to those obtained from the DNS database.

Coupled Map Lattice (CML)

In Chapter 3, the CML equation of Hilgers and Beck [6], [7] that was used to calculate the strain field in this thesis was described. Opposite to the PF model, the CML model simulates velocities from which the strain field has to be calculated. Two independent velocity fields were simulated and assigned arbitrary directions u and v, which are orthogonal to each other. The simulations were run in the $x - y$ space, with parameters $\gamma\tau = 0.02$, $g = 0.0194$, and $C = 1.411$ in Eq. (3.47) and transformed to the $\alpha - \zeta$ space using the mapping rules described in Section 3.6.

Figure 4.5(a) shows the the u-velocity field simulated using the CML model at a level of $k = 3$, which is assumed to be in the integral sub-range of the energy cascade of Fig. 2.1. Figures 4.5(b) and 4.5(c) show the results of the simulation of velocity for levels of $k = 9$ and $k = 15$, respectively. The structures in these figures do not correspond to *eddies*, since *eddies* represent a *vortical* motion and these figures are only a two-dimensional representation of one component of velocity.

A comparison between Figs. 4.5(a), 4.5(b) and 4.5(c) shows that the velocity magnitude decreases about 4 orders of magnitude from levels $k = 3$ to $k = 15$. This proves the capabilities of the model to represent the dissipation of energy from one level to the next. It can also be seen that the structure of the velocity field is more uniform as the k level is increased.

Figures 4.6(a), 4.6(b), and 4.6(c) show the vector form of the two-dimensional velocity fields at different levels of energy for the area delimited by $0.2 < \alpha < 0.6$ and $0.2 < \zeta < 0.6$. The fields were calculated using the results of the simulations of velocities in two orthogonal directions for levels of $k = 3$, $k = 9$, and $k = 15$, respectively.

Comparing these figures, it can be seen that some of the structures present in Fig. 4.6(a) have been completely dissipated, or have been dissipated into smaller structures in Fig. 4.6(c), giving rise to a more orderly field.
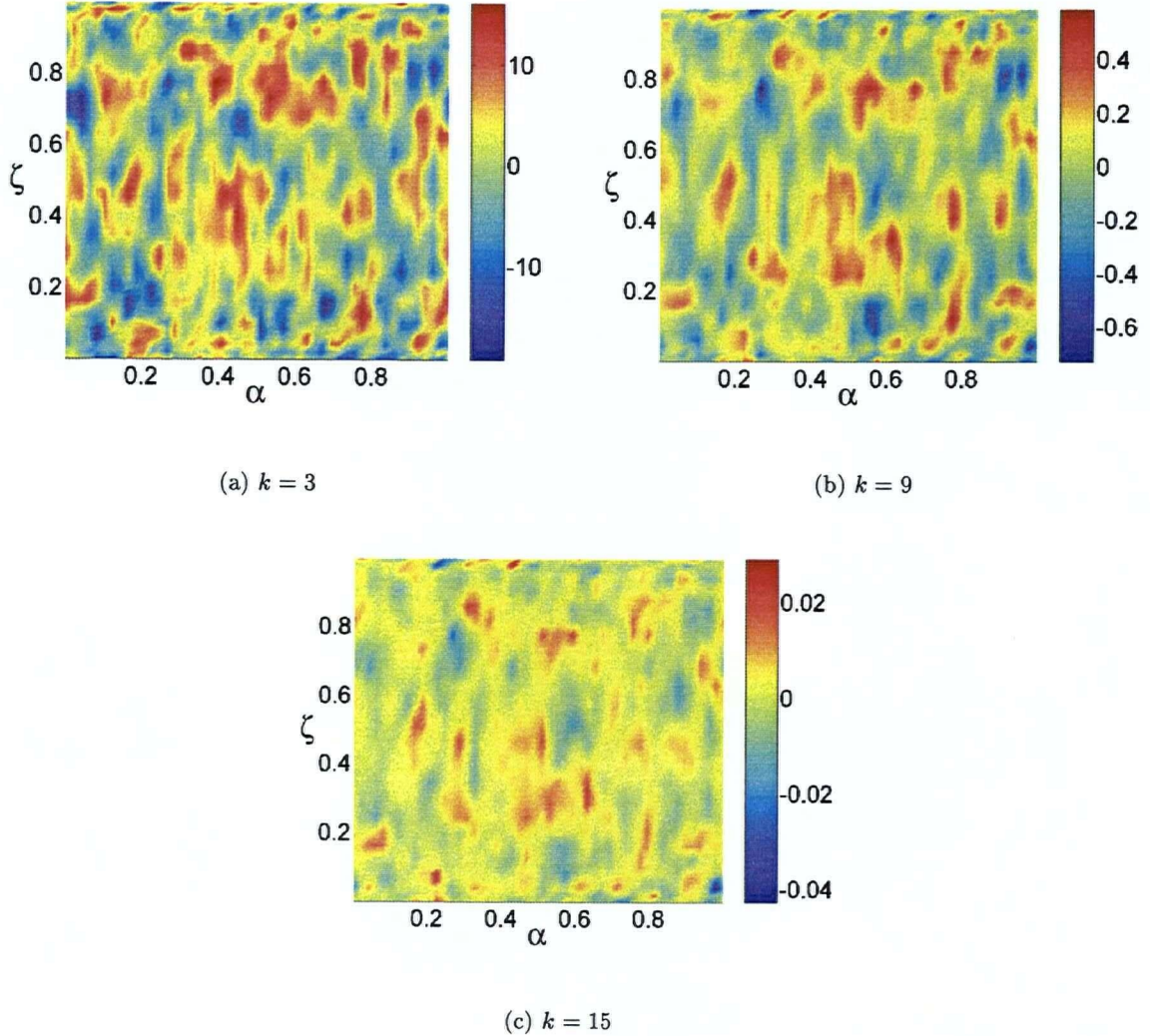

(a) $k = 3$

(b) $k = 9$

(c) $k = 15$

Figure 4.5: u-velocity fields simulated with CML

Figs. 4.7(a), 4.7(b), and 4.7(c) show the strain fields obtained using the CML model and the definition of Eq. (3.48) for energy levels of $k = 3$, $k = 9$, and $k = 15$, respectively. The effects of the decaying energy on the strain fields are evident in these figures. It can be seen that the magnitude of the strain field decays considerably as k advances further into the viscous subrange of the cascade model. This leads to a strain field with fewer peaks and more *neutral*, or *zero-strain* areas as shown in Fig. 4.7(c). Using the values of the turbulence

parameters ϵ and ν from the reference DNS database, it was determined that the level of energy in the CML model that would give the appropriate values corresponds to $k = 9$, which is shown in Fig. 4.7(b).
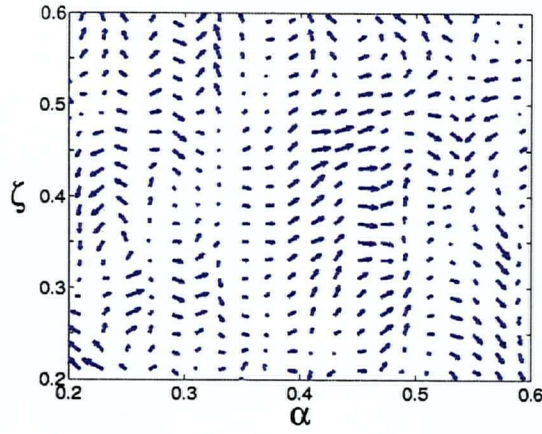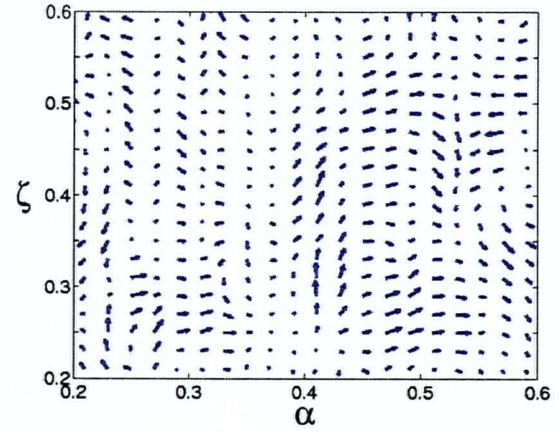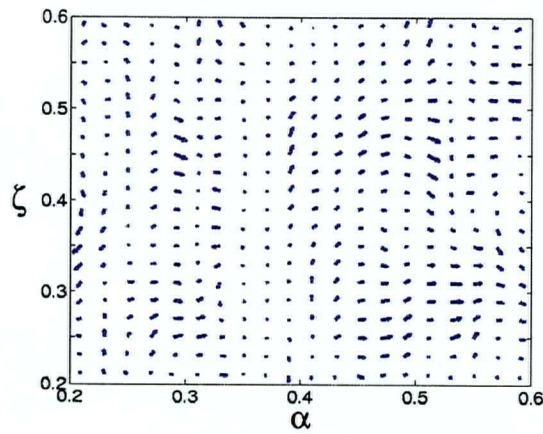

(a) $k = 3$ (b) $k = 9$

(c) $k = 15$
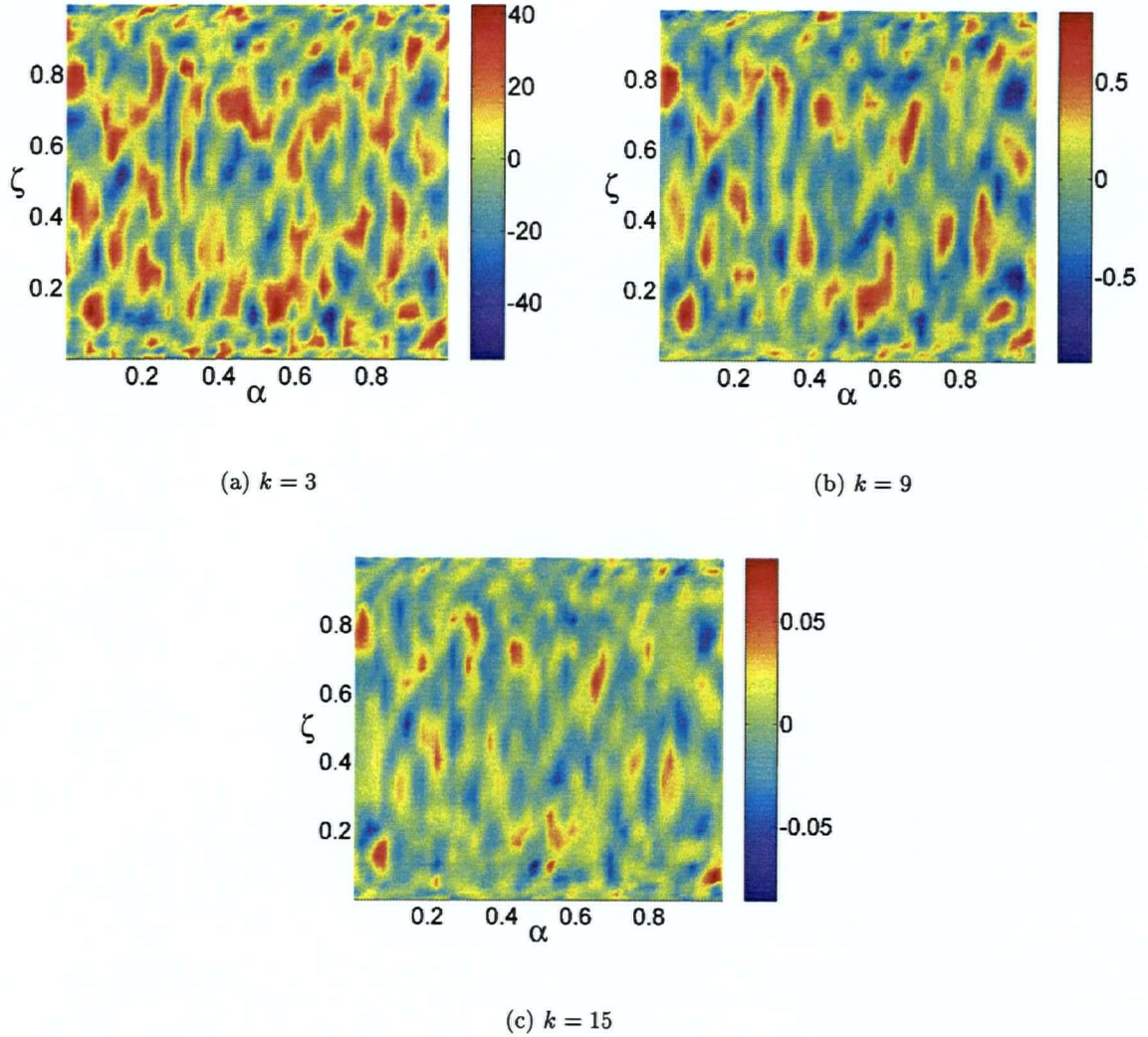
Figure 4.6: Velocity fields simulated with CML

(a) $k = 3$

(b) $k = 9$

(c) $k = 15$

Figure 4.7: Strain fields simulated with CML

Comparing Fig. 4.7(b) with Fig. 4.4(d), it can be seen that there are important differences and similarities between the structure of the fields produced by the PF and the CML models. First, the PF model is based on spectral methods which are inherently *smooth* due to the filtering that occurs as a consequence of Fourier-like transformations. This is proven by the fact that the structures produced by the PF are larger than those simulated with the CML model. It can also be observed that, in general, the fields produced by the PF behave very much as an amplified portion of a selected area of the CML-produced field. This discrepancy could be eliminated by using a larger number of signals in the PF model that would induce more variability along the domain. One of the similarities between the models is their capability to

provide the right orders of magnitude for the field when compared to the calculated value of the strain tensor using ν and ϵ parameters from the DNS database. At $t = 5$ time units, the DNS data yields $S_{ij} = \sqrt{\epsilon/2\nu} = \pm 0.5656$, while the both the CML and PF models provide values in the range $-0.8 < S_{ij} < 0.8$ for the case of $k = 9$, and $\Psi = 5$, respectively.

4.2.2 Predictions of Reactive Scalars

Two different sets of calculations using the PF and CML models proposed in this thesis were performed and compared to the DNS [8] and CMC [9] reference databases. In addition to these, a third set of computations was performed using a generator of Gaussian random numbers that was used in place of the PF and CML models to mimic the chaotic variations of strain. This was done with the objective of determine whether or not a simple set of random numbers would provide similar results to those obtained with the periodic forcing and coupled map lattice models. The results obtained with this scheme are identified as DCMC-RAN in the following figures. Figure 4.8 expresses results in terms of Favre averages which, for the case of species mass fractions, were calculated in a similar fashion as in the CMC formulation as

$$\widetilde{Y} = \frac{\int_0^1 \overline{\rho|\zeta Y|\zeta} P(\zeta) d\zeta}{\int_0^1 \overline{\rho|\zeta} P(\zeta) d\zeta}$$

where $P(\zeta)$ is the PDF of mixture fraction which is represented by the β-PDF taken from the DNS reference database [8].

In Fig. 4.8(a) it can be seen that the DCMC-PF and DCMC-CML models provide predictions of the Favre average of oxidiser mass fraction in excellent agreement with the DNS results with a noticeable improvement over the CMC results, while the DCMC-RAN model provides only a marginal improvement over the CMC predictions. The Favre-averaged methane mass fraction is also well predicted by both the DCMC-PF and DCMC-CML models, as shown in Fig. 4.8(b), with a tendency to under-predict, especially after 35 time units. Figures 4.8(c) and 4.9(a) show that the DCMC-PF and DCMC-CML models provide good predictions of the Favre average and conditionally-averaged intermediate mass fraction after 30.0 time units, respectively. This result has important implications given that the intermediate includes CO. It is expected that if the intermediate mass fraction is properly simulated, the ability to capture its effect in the overall generation of pollutants will be positively affected.
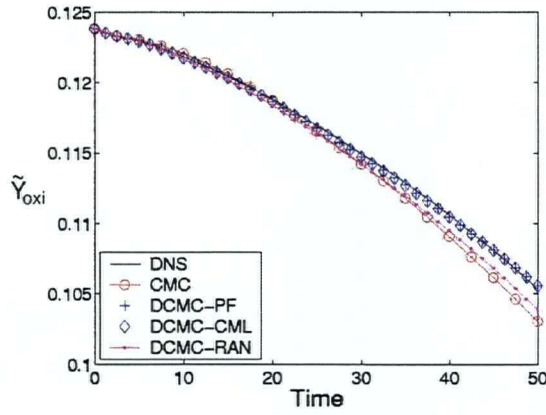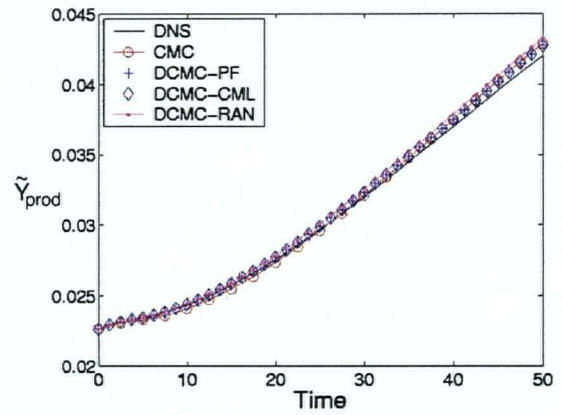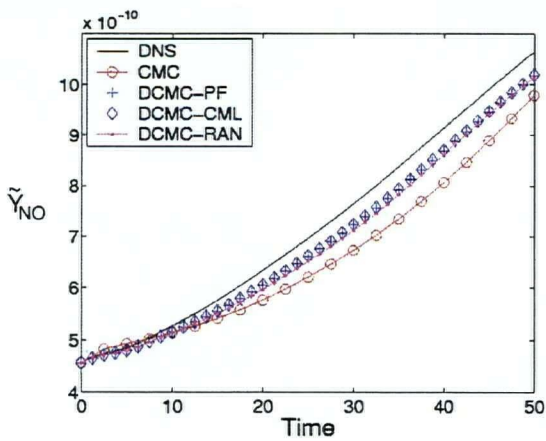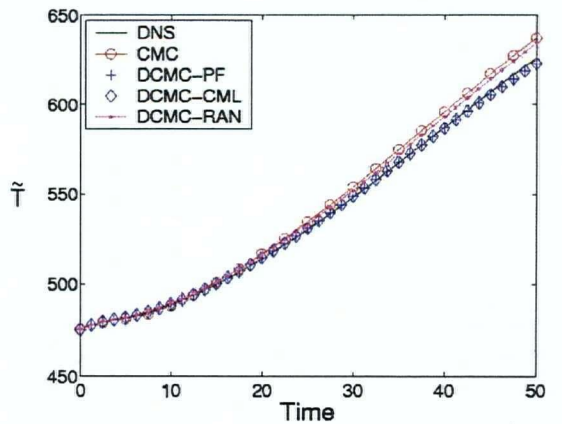
(a) Oxidiser
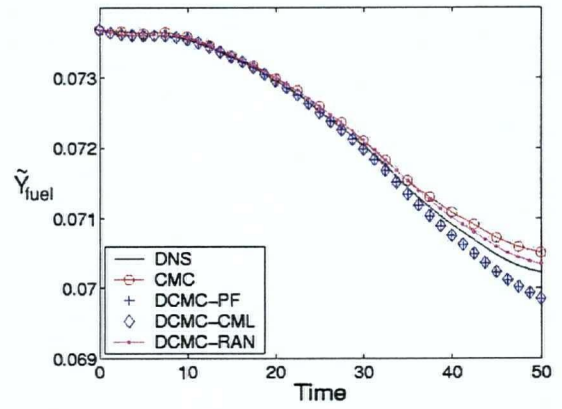
(b) Fuel
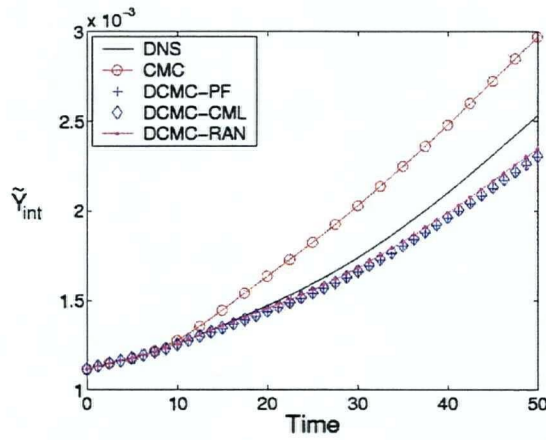
(c) Intermediates

(d) Products

(e) NO

(f) Temperature

Figure 4.8: DNS, CMC, and DCMC Favre averages of species mass fractions

The Favre-averaged mass fraction of products is over-predicted for all times by both DCMC-based simulations as shown in Fig. 4.8(d). This over-prediction, along with the under-prediction of the Favre average of fuel mass fraction, is merely a result of the overprediction of the reaction rates.
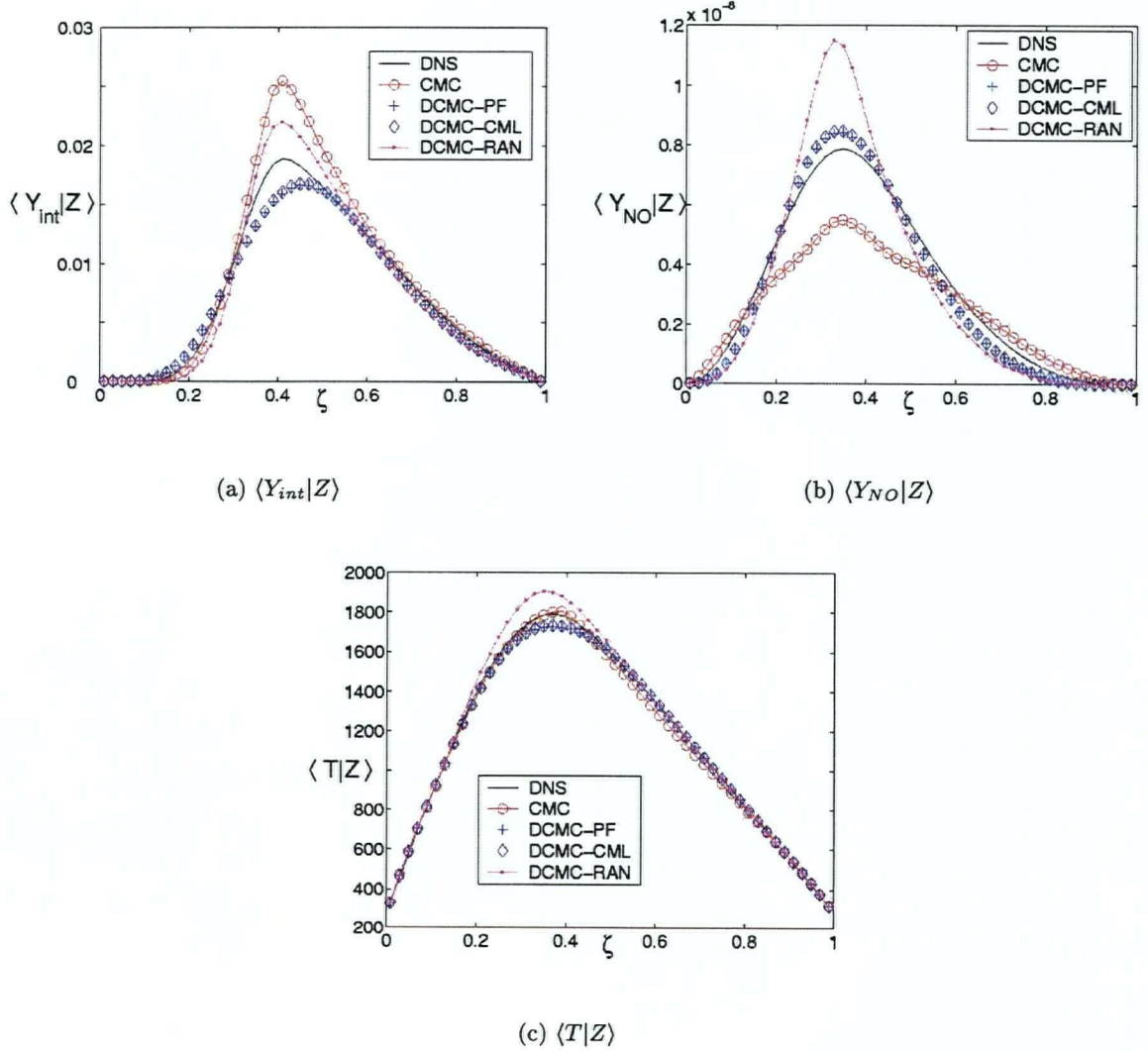

(a) $\langle Y_{int}|Z \rangle$

(b) $\langle Y_{NO}|Z \rangle$

(c) $\langle T|Z \rangle$

Figure 4.9: Conditional averages at t = 30.0

Probably the most significant achievement of this project is the good agreement between the DNS and DCMC-PF and DCMC-CML predictions of NO. Figure 4.8(e) shows an important improvement in the predictions of the Favre average of NO mass fraction over the CMC results. This improvement is also evident in the conditionally-averaged NO mass fraction predictions shown after 30.0 time units in Fig. 4.9(b). The good predictions of NO

mass fraction are closely related to the quality of the predictions of temperature, since the Zel'dovich NO mechanism used to calculate the NO mass fraction is strongly dependent on temperature. Figure 4.8(f) shows the Favre average of temperature, where it can be seen that the DCMC-PF and DCMC-CML results show a considerably improvement in the predicted results over the CMC results. This result is further confirmed by Fig. 4.9(c).
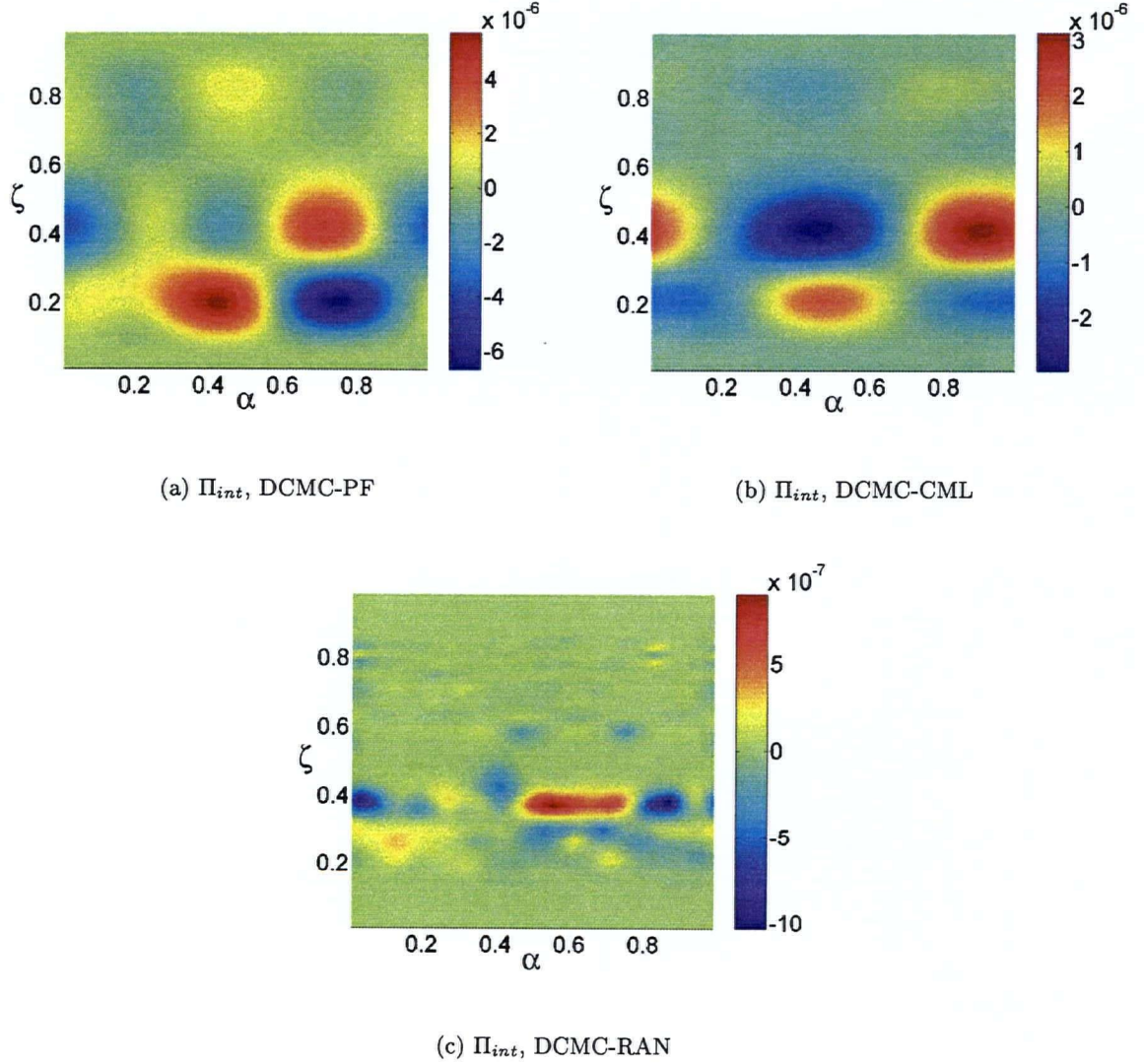

(a) Π_{int}, DCMC-PF

(b) Π_{int}, DCMC-CML

(c) Π_{int}, DCMC-RAN

Figure 4.10: α-variations in the intermediates field at $t = 30.0$

Figures 4.10, 4.11, and 4.12 show comparisons between the variations around the conditional mean in the direction of α for different scalar fields at 30.0 time units calculated with the different models proposed in this research. Here, $\Pi_I = Y_I(\alpha, \zeta) - \langle Y_I | \alpha \rangle$.

(a) Π_{NO}, DCMC-PF

(b) Π_{NO}, DCMC-CML

(c) Π_{NO}, DCMC-RAN
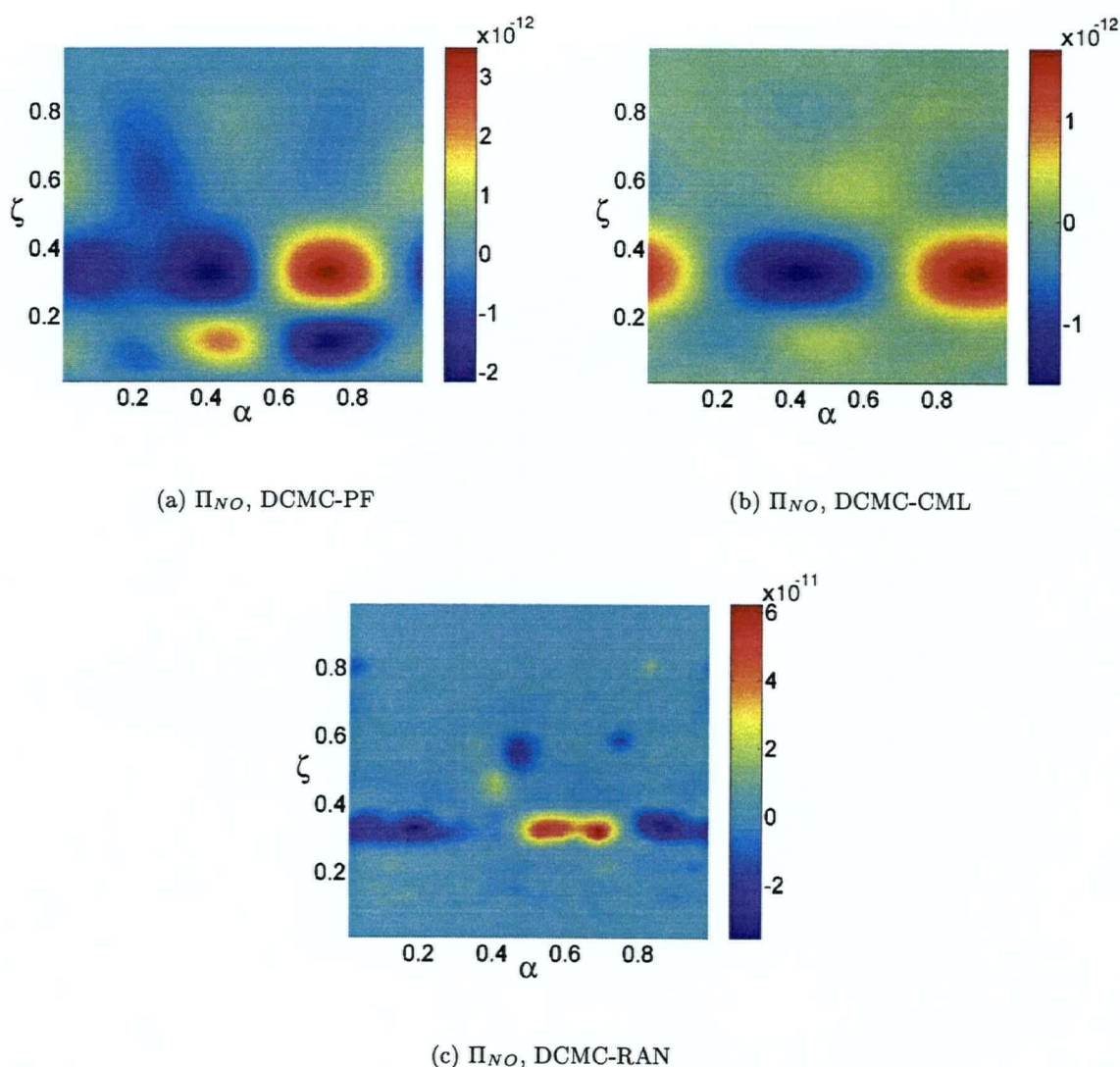
Figure 4.11: α-variations in the NO field at $t = 30.0$

From these figures, it can be seen that the variations simulated by the PF and CML models have similar structures and magnitudes for all cases shown, while the DCMC-RAN implementation simulates variations one order of magnitude smaller in the same fields. For all cases, it is clear that the maximum and minimum variations occur in the vicinity of $\zeta \approx 0.35$, which is where the chemical reaction is assumed to occur with more intensity. While the PF and CML show consistent results with this hypothesis, the RAN implementation shows large variations in the temperature field at a very different location, as shown in Fig. 4.12(c). This is due to the lack of structure in the tensor field calculated with the DCMC-RAN model.

The variations shown in Fig. 4.12(a) and 4.12(b) seem to indicate the presence of extinction and re-ignition phenomena, characterised by 'cold' regions between 'hot' regions. In the case of the figures shown, these variations are rather small, but large enough to produce changes in the simulated values of NO and intermediates, as shown in Fig. 4.11(a), 4.11(b), 4.10(a), and 4.10(b).

Both the PF and RAN simulations took approximately 2.7 hours to complete in a P4 Xeon 2.4 GHz cluster using a single processor, while the CML simulations took approximately 30.0 hours to complete using the same hardware.
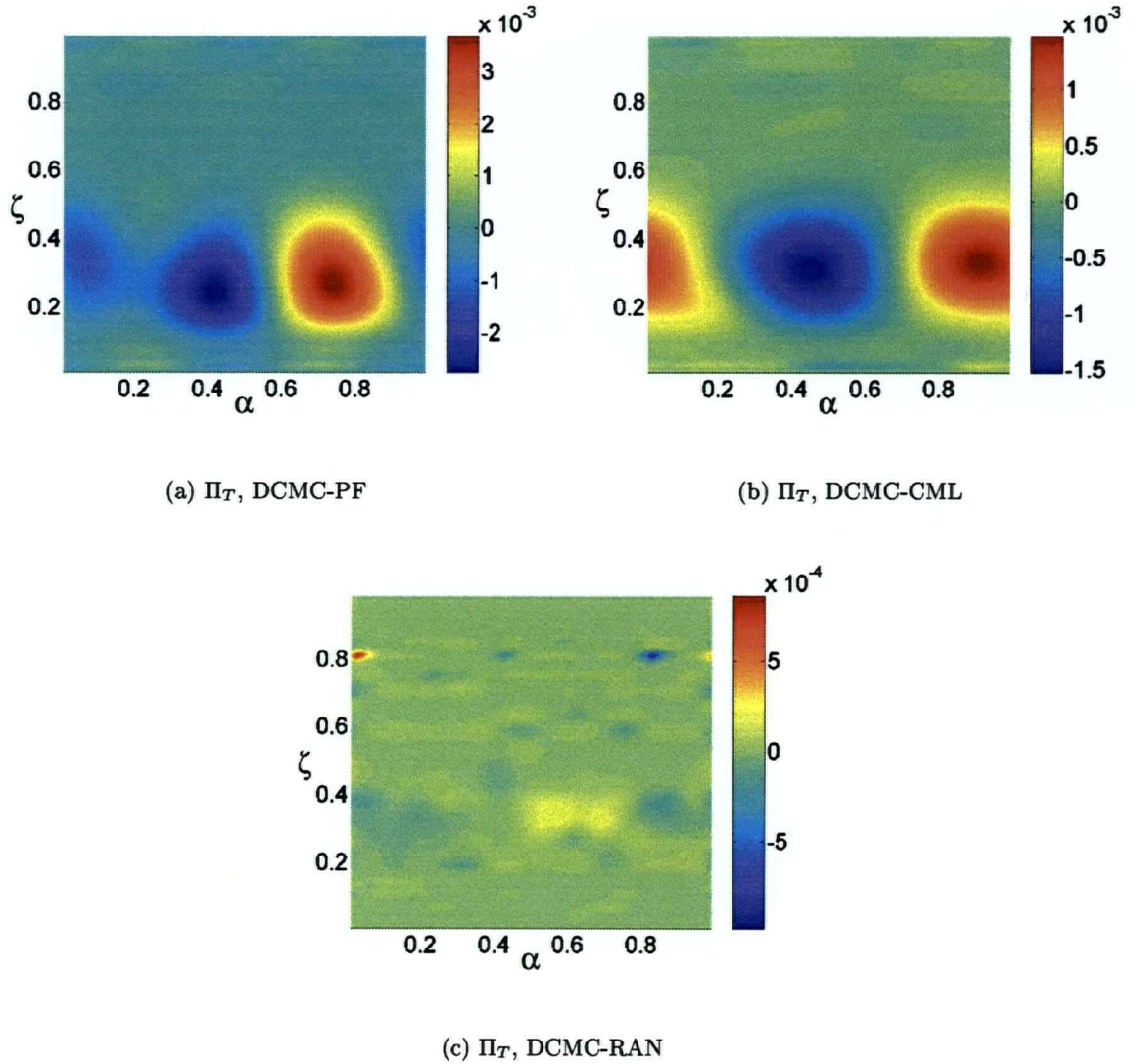

(a) Π_T, DCMC-PF

(b) Π_T, DCMC-CML

(c) Π_T, DCMC-RAN

Figure 4.12: α-variations in the temperature field at $t = 30.0$

4.3　Summary

The results obtained from the numerical implementation of the models proposed in this thesis have been presented in this chapter. The most important observations are summarised as follows:

- The stochastic processes used to simulate the strain tensor proved to offer good results in terms of magnitude and structure of the strain fields. The PF model requires at least 5 signals to offer consistent results, while the CML model provides the structure and magnitude required for the test combustion process at a dissipation level of $k = 9$

- It was observed that by using a second conditional variable additional variations can be simulated with the DCMC model. These variations would have been ignored using the single conditional moment closure.

- In general, the DCMC-PF and DCMC-CML models provided improved predictions of species mass fractions and temperature when compared with the CMC model. This is especially evident in the Favre-averaged predictions of intermediates and NO mass fractions and temperature.

- While the computational expense of the DCMC-RAN is comparable to that of the DCMC-PF model, it was observed that the lack of structure inherent to the RAN implementation results in inconsistent simulations of the scalar fields.

Chapter 5

Conclusions and Recommendations

The application of the DCMC method with stochastic processes to simulate turbulent combustion has been explored throughout the development of this thesis. In this chapter the findings produced with this research are summarised and recommendations for future work are articulated.

The application of stochastic processes and Monte Carlo methods in combustion were described in Chapter 2, along with the general fundamentals of turbulent combustion. Examples of relevant applications to this research were also discussed in Chapter 2.

The derivation of the mathematical models proposed in this thesis took place in Chapter 3. DCMC transport equations of species mass fractions, temperature and scalar dissipation were formulated and the unclosed terms were modelled using two tools: scalar transport and conditional moment closure hypotheses. Two different stochastic processes were also proposed in Chapter 3 of this thesis to model the strain tensor in the transport equation of scalar dissipation.

The numerical implementation of the models developed in Chapter 3 showed encouraging results in terms of simulations of the strain tensor, as well as predictions of temperature and intermediates and NO mass fraction. The addition of the second scalar variable induced variations that cannot be simulated by the single conditional moment closure method. These results are discussed and summarised in Chapter 4.

An example of the applicability and advantages of the DCMC method with stochastic processes in simulation of turbulent combustion has been demonstrated with the results obtained from this research. As with many other projects, however, areas of improvement have

also been identified that would make the model more robust and applicable to a more general range of problems. It is then proposed to:

- Explore ways in which this or a similar model could work linked to a CFD program. With this model it is possible to use the fluid flow data provided by a CFD program as a real-time input. The code would then calculate the strain field and the solution for Eq. 4.1, returning updated values of density, temperature, viscosity, etc. to the CFD code.

- Investigate the effects of increased variations around the conditional mean of a. These variations could be induced by modifying the initial conditions and coupling between the scalar dissipation of a and Z.

- Investigate the use of the models presented in this thesis including variations in space. This implies a different approach for the closure of Eqs. (3.20) and (3.21) to that presented in Chapter 3. It is possible that the differences between the results presented in this research and those found in the DNS reference database could be due to the lack of a spatial variable. The use of such as a conditional variable will provide the model with a capability to discriminate among isosurfaces of mixture fraction and a.

- Test a different case. As with most numerical models, it is important to verify the validity and applicability of the hypotheses used in the development of the model. The combustion of Hydrogen-Oxygen and Hydrogen-Air flames has been studied extensively and could present itself as a good candidate for comparison purposes with the models presented in this thesis.

Bibliography

[1] N. Peters, Turbulent Combustion, Cambridge University Press, 2000.

[2] J. Warnatz, U. Maas, R. W. Dibble, Combustion. Physical and Chemical Fundamentals, Modeling and Simulation, Experiments, Pollutant Formation, Springer, 2001.

[3] A. Y. Klimenko, Multicomponent diffusion of various admixtures in turbulent flow, Fluid Dynamics 25 (1990) 327–334.

[4] R. W. Bilger, Conditional moment closure for turbulent reacting flow, Phys. Fluids 5 (2) (1993) 436–444.

[5] C. Beck, Chaotic cascade model for turbulent velocity distributions, Physical Review E 49 (5) (1994) 3641–3652.

[6] A. Hilgers, C. Beck, Coupled map lattices simulating fully developed turbulent flows, AIP Conference Proceedings 411 (1997) 11–17.

[7] A. Hilgers, C. Beck, Hierarchical coupled map lattices as cascade models for hydrodynamical turbulence, Europhysics Letters 45 (5) (1999) 552–557.

[8] W. K. Bushe, R. W. Bilger, G. R. Ruetsch, Incorporating realistic chemistry into direct numerical simulations of turbulent non-premixed combustion, in: Annual Research Briefs. Center for Turbulence Research, NASA Ames/Stanford University, 1997, pp. 195–211.

[9] W. K. Bushe, R. W. Bilger, Conditional moment closure modeling of turbulent non-premixed combustion with reduced chemistry, in: Annual Research Briefs. Center for Turbulence Research, NASA Ames/Stanford University, 1999, pp. 139–154.

[10] D. Veynante, L. Vervisch, Turbulent combustion modeling, Progress in Energy and Combustion Science 28 (2002) 193–266.

[11] F. A. Williams, Combustion Theory, Addison-Wesley Publishing Company, Inc., 1985.

[12] N. Peters, Reduced kinetic mechanisms and assymptotic approximations for methane-air flames, Springer, 1991, Ch. Reducing mechanisms, pp. 48–67.

[13] R. W. Bilger, M. B. Esler, S. H. Starner, Reduced kinetic mechanisms and assymptotic approximations for methane-air flames, Springer, 1991, Ch. On reduced mechanisms for methane-air combustion, pp. 86–110.

[14] H. Tennekes, J. L. Lumley, A First Course in Turbulence, The MIT Press, 1992.

[15] A. N. Kolmogorov, The local structure of turbulence in incompressible viscous fluid for very large reynolds numbers, Dokl. Akad. Nauk. SSSR 30 (4) (1941) 3201.

[16] W. K. Bushe, Conditional Moment Closure Methods for Autoignition Problems. PhD. Thesis, University of Cambridge, 1996.

[17] B. E. Launder, D. B. Spalding, Lectures in Mathematical Models of Turbulence, Academic Press, 1972.

[18] S. B. Pope, Turbulent Flows, Cambridge University Press, 2000.

[19] T. B. Gatski, C. L. Rumsey, Closure Strategies for Turbulent and Transitional Flows, Cambridge University Press, 2002, Ch. Linear and Nonlinear Eddy Viscosity Models, pp. 9–46.

[20] W. K. Bushe, Combustion Lecture Notes, University of British Columbia, 2003.

[21] W. E. Mell, V. Nilsen, G. Kosály, J. J. Riley, Investigation of closure models for non-premixed turbulent reacting flows, Phys. Fluids 6 (3) (1994) 1331–1356.

[22] N. Swaminathan, R. W. Bilger, Assessment of combustion submodels for turbulent non-premixed hydrocarbon flames, Combustion and Flame 116 (1999) 519–545.

[23] R. W. Bilger, Future progress in turbulent combustion research, Prog. Energy Combust. Sci. 26 (2000) 367–380.

[24] T. Echekki, C. J. H., Unsteady strain rate and curvature effects in turbulent premixed methane-air flames, Combustion and Flame 106 (1995) 184–202.

[25] H. Pitsch, H. Steiner, Large-eddy simulation of a piloted methane/air diffusion flame (sandia flame d), Phys. Fluids 12 (10) (2000) 2541–2554.

[26] H. Steiner, W. K. Bushe, Large-eddy simulation of a turbulent reacting jet with conditional source-term estimation, Phys. Fluids 13 (3) (2001) 754–769.

[27] D. Laurence, Closure Strategies for Turbulent and Transitional Flows, Cambridge University Press, 2002, Ch. Large Eddy Simulation of Industrial Flows?, pp. 392–406.

[28] N. Peters, Laminar diffusion flamelet models in non-premixed turbulent combustion, Energy Combust. Sci. 10 (1984) 319–339.

[29] D. Lentini, Assessment of the stretched laminar flamelet approach for nonpremixed turbulent combustion, Combust. Sci. and Tech. 100 (1994) 95–122.

[30] A. W. Cook, J. J. Riley, G. Kosály, A laminar flamelet approach to subgrid-scale chemistry in turbulent flows, Combustion and Flame 109 (1997) 332–341.

[31] F. Mauss, D. Keller, N. Peters, A lagrangian simulation of flamelet extinction and re-ignition in turbulent jet diffusion flames, in: Twenty-Third Symposium (International) on Combustion. The Combustion Institute, 1990, pp. 693–698.

[32] H. Pitsch, Unsteady flamelet modeling of differential diffusion in turbulent jet diffusion flames, Combustion and Flame 123 (2000) 358–374.

[33] W. P. Jones, Closure Strategies for Turbulent and Transitional Flows, Cambridge University Press, 2002, Ch. The Joint Scalar Probability Density Function Method, pp. 582–625.

[34] A. Einstein, Über die von der molekularkinetischen theorie der wärme geforderte bewegung von in ruhenden flüssigkeiten suspendierten teilchen, Annalen der Physik 4 (17) (1905) 549–561.

[35] A. Einstein, Investigations on the theory of the Brownian movement. Ed. R. Fürth, Tr. A. D. Cowper, Methuen, 1926.

[36] M. von Smoluchowski, Zur kinetischen theorie der brownschen molekularbewegung und der suspensionen, Annalen der Physik 4 (21) (1906) 756–781.

[37] P. Langevin, Sur la théorie du mouvement brownien, Comptes Rendus de l'Académie des Sciences (Paris) 146 (1908) 530.

[38] J. B. Perrin, La discontinuité de la matière, Revue du Mois 1 (1909) 323–344.

[39] J. B. Perrin, Mouvement brownien et réalité moléculaire, Annales de chimie et de physiqe VIII (18) (1909) 5–114.

[40] J. B. Perrin, Brownian Movement and Molecular Reality, Taylor and Francis, 1909.

[41] J. B. Perrin, Les Atomes, Alcan, 1913.

[42] J. B. Perrin, Atoms. Tr. D. L. Hammick, Constable, 1970.

[43] P. R. Kramer, A review of some monte carlo simulation methods for turbulent systems, Lecture Notes, Department of Mathematical Sciences, Rensselaer Polytechnic Institute .

[44] F. W. J. Elliot, D. Horntrop, A. J. Majda, A fourier-wavelet monte carlo method for fractal random fields, J. Comp. Phys. 132 (2) (1997) 384–408.

[45] K. K. Sabelfeld, Monte Carlo methods in boundary value problems, Springer-Verlag, 1991.

[46] A. McCoy, PhD Thesis, Department of Mathematics, University of California at Berkeley, 1975.

[47] J. P. Minier, J. Pozorski, Wall-boundary conditions in probability density function methods and applications to a turbulent channel flow, Phys. Fluids 11 (9) (1999) 2632–2644.

[48] W. C. Welton, Two-dimensional pdf/sph simulations of compressible turbulent flows, J. Comput. Phys. 139 (2) (1998) 410–443.

[49] D. J. Thomson, Criteria for the selection of stochastic models of particle trajectories in turbulent flows, J. Fluid Mech. 180 (1987) 529–556.

[50] J. Pozorski, J. P. Minier, Probability density function modeling of dispersed two-phase turbulent flows, Phys. Rev. E 59 (1) (1999) 855.

[51] F. A. Jaberi, P. J. Colucci, S. James, P. Givi, S. B. Pope, Filtered mass density function for large-eddy simulation of turbulent reacting flows, J. Fluid Mech. 401 (1999) 85–121.

[52] A. Obieglo, J. Gass, D. Poulikakos, Comparative study of modeling a hydrogen non-premixed turbulent flame, Combust. Flame 122 (2000) 176–194.

[53] O. Le Maitre, O. M. Knio, H. N. Najm, R. G. Ghanem, A stochastic projection method for fluid flow: I. basic formulation, J. Comp. Phys. 173 (2001) 481–511.

[54] S. B. Pope, A monte carlo method for the pdf equations of turbulent reactive flow, Comb. Sci. Tech. 25 (1981) 159–174.

[55] E. E. O'Brien, The Probability Density Function (pdf) Approach to Reacting Turbulent Flows, Springer-Verlag, 1980.

[56] R. G. Batt, Turbulent mixing in a low speed shear layer., J. Fluid Mech. 82 (1977) 53.

[57] L. Valiño, A field monte carlo formulation for calculating the probability denstity function of a single scalar in a turbulent flow, Flow, Turb. Comb. 60 (1998) 157–172.

[58] T. Hulek, R. P. Lindstedt, Modelling unclosed nonlinear terms in a pdf closure for turbulent flames, Math. Comp. Modelling 24 (8) (1996) 137–147.

[59] T. Hulek, L. R. P., Computation of steady-state and transient premixed turbulent flames using pdf methods, Comb. Flame 104 (1996) 481–504.

[60] H. Kawanabe, M. Shioji, M. Ikegami, Cfd simulation for turbulent mixing with the stochastic approach, Heat Transf. A. Res. 30 (6) (2001) 503–511.

[61] S. M. Cannon, B. S. Brewster, L. D. Smoot, Stochastic modeling of co and no in premixed methane combustion, Comb. Flame 113 (1998) 135–146.

[62] M. Kraft, F. Harald, Some analytic solutions for stochastic reactor models based on the joint composition pdf, Comb. Theory Mod. 3 (1999) 343–358.

[63] C. Cha, G. Kosàly, H. Pitsch, Modeling extinction and reignition in turbulent non-premixed combustion using a doubly-conditional closure approach., Physics of Fluids 13 (12) (2001) 3824–3834.

[64] N. B. Vargaftik, Tables on the Thermophysical Properties of Liquids and Gases, John Wiley and Sons, 1975.

[65] V. Eswaran, S. B. Pope, Direct numerical simulations of the turbulent mixing of a passive scalar, Phys. Fluids 31 (3) (1988) 506–520.

[66] U. C. Müller, N. Peters, Development of reduced reaction schemes for the ignition of diesel fuels in a non-premixed turbulent flow field, IDEA-Programme Internal Report .

[67] D. Thévenin, S. Candel, Effect of variable strain on the dynamics of diffusion flame ignition, Combust. Sci. and Tech. 91 (1993) 73–94.

[68] E. Mastorakos, T. A. Baritaud, T. J. Poinsot, Numerical simulations of autoignition in turbulent mixing flows, Combust. Sci. and Technol. 125 (1997) 243–282.

[69] G. R. Ruetsch, M. R. Maxey, Small-scale features of vorticity and passive scalar fields in homogeneous isotropic turbulence, Phys. Fluids 3 (6) (1991) 1587–1597.

[70] T. S. Cheng, J. A. Wehrmeyer, R. W. Pitz, O. Jarrett, G. B. Northam, Finite-rate chemistry effects in a mach 2 reacting flow, AIAA/ASME/SAE 27th Joint Propulsion Conference .

[71] H. Pitsch, S. Fedotov, Investigation of scalar dissipation rate fluctuations in non-premixed turbulent combustion using a stochastic approach, Combustion Theory and Modelling 5 (2001) 41–57.

[72] S. A. Orszag, G. S. Patterson, Statistical models and turbulence, lecture notes in Physics, Springer, 1972, Ch. Numerical simulation of turbulence.

[73] V. Eswaran, S. B. Pope, An examination of forcing in direct numerical simulations of turbulence, Comput. Fluids 16 (3) (1988) 257–278.

[74] A. Hilgers, M. Gremm, J. Schnakenberg, A criterion for stochastic resonance, Physics Letters A 209 (1995) 313–316.

[75] F. A. Williams, Reduced kinetic mechanisms and assymptotic approximations for methane-air flames, Springer, 1991, Ch. Overview of asymptotics for methane flames.

[76] N. Swaminathan, R. W. Bilger, Direct numerical simulation of turbulent nonpremixed hyrdocarbon reaction zones using a two-step reduced mechanism, Combust. Sci. Tech. 127 (1998) 167.

[77] P. N. Brown, G. D. Byrne, A. C. Hindmarsh, Vode: A variable coefficient ode solver, SIAM J. Sci. Stat. Comput. 10 (1989) 1038–1051.

[78] W. K. Bushe, R. S. Cant, Results of direct numerical simulations of premixed combustion, in: Cambridge University Engineering Department Internal Report CUED/A-THERMO/TR63, 1996.